J. Fluid Mech. (1993), *vol.* 247, *pp.* 551–588

Infragravity waves induced by short-wave groups

By HEMMING A. SCHÄFFER

Danish Hydraulic Institute, Agern Allé 5, DK-2970 Hørsholm, Denmark

(Received 25 November 1991 and in revised form 8 September 1992)

A theoretical model for infragravity waves generated by incident short-wave groups is developed. Both normal and oblique short-wave incidence is considered. The depth-integrated conservation equations for mass and momentum averaged over a short-wave period are equivalent to the nonlinear shallow-water equations with a forcing term. In linearized form these equations combine to a second-order long-wave equation including forcing, and this is the equation we solve. The forcing term is expressed in terms of the short-wave radiation stress, and the modelling of these short waves in regard to their breaking and dynamic surf zone behaviour is essential. The model takes into account the time-varying position of the initial break point as well as a (partial) transmission of grouping into the surf zone. The former produces a dynamic set-up, while the latter is equivalent to the short-wave forcing that takes place outside the surf zone. These two effects have a mutual dependence which is modelled by a parameter κ, and their relative strength is estimated. Before the waves break, the standard assumption of energy conservation leads to a variation of the radiation stress, which causes a bound, long wave, and the shoaling bottom results in a modification of the solution known for constant depth. The respective effects of this incident bound, long wave and of oscillations of the break-point position are shown to be of the same order of magnitude, and they oppose each other to some extent. The transfer of energy from the short waves to waves at infragravity frequencies is analysed using the depth-integrated conservation equation of energy. For the case of normally incident groups a semi-analytical steady-state solution for the infragravity wave motion is given for a plane beach and small primary-wave modulations. Examples of the resulting surface elevation as well as the corresponding particle velocity and mean infragravity-wave energy flux are presented. Also the sensitivity to the variation of input parameters is analysed. The model results are compared with laboratory experiments from the literature. The qualitative agreement is good, but quantitatively the model overestimates the infragravity wave activity. This can, in part, be attributed to the neglect of frictional effects.

1. Introduction

The irregularities present in any natural wavetrain are responsible for higher-order fluctuations of the mean water surface. Particularly when the waves have a pronounced grouping, these fluctuations appear as long waves at the group frequency, and it is the purpose of the present work to study this long-wave motion in the nearshore. Typically the periods of this motion are of the order of several minutes, and the term *infragravity waves* has become customary for the phenomenon. The original term *surf beats* was used by Munk (1949) and Tucker (1950), who were probably the first to report field measurements of this kind of oscillation. Both these authors observed low-frequency disturbances, which were apparently correlated to

groups of high waves after a time lag, approximately equal to the time required for the waves to travel from the wave recorder to the coastline, and return at the long-wave speed.

In the early sixties Longuet-Higgins & Stewart (1962, 1964) developed the theory of *radiation stress*, by which they explained how groups of high waves are accompanied by a depression of the mean water surface. In other words, groups of short waves *force* a long wave, which is known as the set-down (wave) or the bound, long wave. Because of the time lag the low-frequency oscillations observed by Munk and Tucker could not be explained as the bound, long wave itself, but rather as its reflection from the coastline once it was released owing to the short-wave breaking.

In recent decades numerous observations have shown that the energy at surf beat frequencies can be substantial, and in some cases even exceed that of the short waves (Wright, Guza & Short 1982). Likewise, the shoreline amplitudes arising from infragravity waves can be comparable to the run-up height of the short waves (Guza & Thornton 1982, 1985).

Symonds, Huntley & Bowen (1982) were the first to consider the effect of oscillations of the break-point position, and they showed that this provides a mechanism of infragravity wave generation in addition to the direct forcing from short-wave grouping. Related works are the numerical approaches of Lo (1988), Nakaza & Hino (1991), and Roelvink (1991) and the spectral model of Van Leeuwen & Battjes (1990). Furthermore, Symonds & Bowen (1984) extended the work of Symonds *et al.* (1982) to include an offshore bar.

Theories concerning offshore long-wave generation by short-wave groups are also relevant to the present work. In the open sea Molin (1982) showed that for deep-water short waves the passage of groups over discontinuities in the bottom slope results in the emission of free, long waves in addition to the bound, long waves that are present. Mei & Benmoussa (1984) generalized these results to obliquely incident groups and an arbitrary depth relative to the short-wave motion. The equations behind this work came from a WKB-expansion by Chu & Mei (1970), and they are equivalent to the conservation equations of mass and momentum also used by Symonds *et al.* (1982). Liu (1989) suggested a different method of solution and gave corrections to the boundary conditions used by Mei & Benmoussa.

With the restriction of constant depth, other related works are Bowers (1977), who showed that bound, long waves are a possible source of harbour resonance (see also the more recent developments by Mei & Agnon 1989; Wu & Liu, 1990); Ottesen Hansen (1978), who treated long waves forced by a spectrum of short waves; and Sand (1982), who analysed the impact of these long waves on laboratory models, see also the recent development by Schäffer (1993).

In the present work we use the linearized depth-integrated conservation equations for mass and momentum which combine to a second-order long-wave equation with a forcing term (Symonds *et al.* 1982 and others). The forcing term is expressed in terms of the short-wave radiation stress, and the modelling of these short waves in regard to their breaking and surf zone dynamics is essential. The model takes into account the time-varying position of the initial break point as well as a (partial) transmission of grouping into the surf zone. The basic formulation (§2 and §3) is given for both normal and oblique incidence of the short-wave groups, whereas the solution is confined to normal incidence for a one-dimensional topography.

In §2 we formulate the governing equation for the infragravity waves and introduce a new modelling of the surf zone dynamics for incident groups.

Section 3 concerns the transfer of energy from the short waves to waves at

infragravity frequencies. This involves the depth-integrated conservation equation of energy.

For normally incident groups with small modulations a semi-analytical steady-state solution for the infragravity wave motion on a plane beach is given in §4, and in a number of examples the resulting surface elevation as well as particle velocity and the mean infragravity-wave energy flux are presented. The results are compared with the theory of Symonds *et al.* (1982) and with laboratory experiments of Kostense (1984). Solutions for oblique short-wave incidence including resonant edge wave exitation will be given in a later publication.

2. Mathematical model

2.1. *Infragravity wave motion*

The phenomenon of infragravity waves forced by short waves involves two scales in time as well as in space. Typically, the timescale of the short waves is $O(10\text{ s})$ and of the infragravity waves $O(100\text{ s})$. One way to treat this problem is to separate the two scales explicitly as in a WKB-expansion. Here we shall use another approach, which is perhaps less stringent, but probably more transparent, physically as well as mathematically. Regardless of the approach the same equations result.

From the 'narrow-minded' short-wave point of view the infragravity motion is merely a slowing varying current and depth. In comparison with the large lengthscale of the infragravity wave, the water will be shallow, and accordingly the current will be uniform over depth. Thus we can use the depth-integrated and time-averaged conservation equations of mass and momentum for waves on a slowly varying uniform current, where the time-averaging is taken over one short-wave period.

Tensor notation with the usual summation convention for double indices is used in this chapter, and the axes of a horizontal Cartesian coordinate system x_i, $i = 1, 2$ are also referred to as $x = x_1$ and $y = x_2$.

2.1.1. *Governing equations*

Following Phillips (§3.6, 1977) we have conservation of mass:

$$\frac{\partial \overline{\zeta}}{\partial t} + \frac{\partial \overline{Q}_i}{\partial x_i} = 0, \tag{2.1}$$

and conservation of momentum:

$$\frac{\partial \overline{Q}_i}{\partial t} + \frac{\partial}{\partial x_j}\left(\frac{\overline{Q}_i \overline{Q}_j}{h+\overline{\zeta}} + \frac{S_{ij}}{\rho}\right) + g(h+\overline{\zeta})\frac{\partial \overline{\zeta}}{\partial x_i} = 0, \tag{2.2}$$

see figure 1 for definitions. Here $\overline{Q}_i$ is the total volume flux defined as the sum of the (mean) volume flux $Q_{s,i}$ of the short waves, and the volume flux of the current $Q_{c,i} = (h+\overline{\zeta})U_{c,i}$

$$\overline{Q}_i = Q_{s,i} + Q_{c,i}, \tag{2.3}$$

where $U_{c,i} = U_{c,i}(x_i, t)$ is the uniform current under wave trough level assumed in the derivation of (2.1) and (2.2). This current is allowed to have a small variation in time as well as in space, and together with $\overline{\zeta}$ it describes the low-frequency motion under investigation. Further S_{ij} is the radiation stress, ρ is density, and g is acceleration of gravity. Defining the mean horizontal velocities by

$$(U_i, U_{s,i}, U_{c,i}) \equiv \frac{1}{h+\overline{\zeta}}(\overline{Q}_i, Q_{s,i}, Q_{c,i}), \tag{2.4}$$

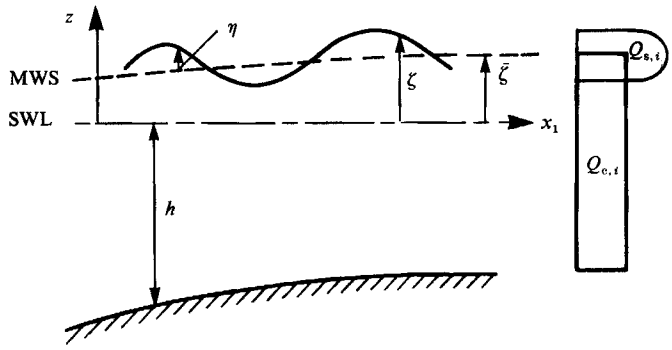

FIGURE 1. Definition sketch. Vertical cross-section along x_i.

where $U_{s,i}$ and $U_{c,i}$ are given for later use, equations (2.1) and (2.2) can be written as

$$\frac{\partial \bar{\zeta}}{\partial t}+\frac{\partial}{\partial x_i}[(h+\bar{\zeta})U_i]=0, \tag{2.5}$$

and

$$\frac{\partial U_i}{\partial t}+U_j\frac{\partial U_i}{\partial x_j}+g\frac{\partial \bar{\zeta}}{\partial x_i}=-\frac{1}{\rho}\frac{1}{h+\bar{\zeta}}\frac{\partial S_{ij}}{\partial x_j}, \tag{2.6}$$

which are the nonlinear shallow-water equations with a forcing term.

Once the forcing term is known from the short waves, the surf beat wave can, in principle, be found by solving (2.5) and (2.6) simultaneously, subject to relevant boundary (and initial) conditions. However, the forcing term itself depends weakly on the solution through the total water depth $h+\bar{\zeta}$ and the interaction between the short waves and the current corresponding to the surf beat wave. When the equations are linearized, this dependency vanishes, since we get

$$\frac{\partial \bar{\zeta}}{\partial t}+\frac{\partial}{\partial x_i}(hU_i)=0, \tag{2.7}$$

and

$$\frac{\partial U_i}{\partial t}+g\frac{\partial \bar{\zeta}}{\partial x_i}=-\frac{1}{\rho h}\frac{\partial S_{ij}}{\partial x_j}. \tag{2.8}$$

In this formulation the undisturbed depth h is consequently used in the calculation of the radiation stress, where also the current interaction is neglected. Eliminating U_i from (2.7) and (2.8) we get

$$\frac{\partial}{\partial x_i}\left(gh\frac{\partial \bar{\zeta}}{\partial x_i}\right)-\frac{\partial^2 \bar{\zeta}}{\partial t^2}=-\frac{1}{\rho}\frac{\partial^2 S_{ij}}{\partial x_i \partial x_j} \tag{2.9}$$

which is the linear shallow-water equation with a forcing term. This linear equation was also obtained by Mei & Benmoussa (1984; note that in their equation (2.11) the minus sign on the right-hand side is missing) using a WKB-expansion from Chu & Mei (1970). In order to describe the nonlinearity of the infragravity waves as in (2.1) and (2.2) or (2.5) and (2.6), this expansion would have to be carried to a higher order.

For a uniform beach slope Carrier & Greenspan (1958) solved the nonlinear shallow-water equations for cross-shore free, long waves and found that, although the solution for the surface elevation close to the shoreline was very different from

the linear solution, the run-up height was the same as predicted from the linearized equations. This gives a little comfort when dealing with the linear theory.

A well-known solution to (2.9) is the bound, long wave described by Longuet-Higgins & Stewart (1962, 1964) for constant depth.

2.1.2. *Boundary conditions*

At the coastline we shall assume full reflection of infragravity waves. In the limit of $h \to 0$ (i.e. at the coastline) this condition gives a standing wave, but because of the forcing that takes place we cannot expect a pure standing wave away from the coastline. The solution to (2.9) can be expressed as

$$\bar{\zeta} = \alpha \bar{\zeta}^{(1)} + \beta \bar{\zeta}^{(2)} + \bar{\zeta}_{\mathrm{p}}, \tag{2.10}$$

where $\bar{\zeta}^{(1)}$ and $\bar{\zeta}^{(2)}$ are the two linearly independent homogeneous solutions, and $\bar{\zeta}_{\mathrm{p}}$ is a particular solution, which is conveniently chosen so that it vanishes at the coastline. In a complex representation, where $\bar{\zeta}^{(1)}$ and $\bar{\zeta}^{(2)}$ are free, long waves travelling in opposite directions, the condition that $\bar{\zeta}$ must be non-singular at the shoreline boundary gives

$$\alpha = \beta, \tag{2.11}$$

provided that $|\bar{\zeta}^{(1)}| = |\bar{\zeta}^{(2)}|$.

The verbal formulation of the seaward boundary condition is dependent on the behaviour of the solution far offshore. If the solution here is oscillatory, we specify that there are no incident free, long waves, and if it is exponential, we require the solution to be evanescent, which rules out exponential seaward growth. However, we can choose the solution so that these conditions have the same mathematical formation. In a complex representation where $\bar{\zeta}^{(1)}$ is a seaward propagating (oscillatory) wave we require $\beta = 0$ (no incoming free, long waves). (Here α and β are different from those at the coastline since they correspond to solutions in different regions (see the matching conditions).) However, if the incoming short-wave conditions are changed so that the solution becomes exponential, then $\bar{\zeta}^{(1)}$ becomes real and evanescent and $\beta = 0$ is still the right condition.

2.1.3. *Matching conditions*

It appears later that we shall have to match the solutions along the common boundary of two regions, for example, inside and outside the break point. Only one-dimensional topography will be considered and matching will only be relevant at lines parallel with the shoreline $x = x_{\mathrm{m}}$, where the subscript m refers to the matching. Since (2.9) is a second-order differential equation, two matching conditions are needed. One is obtained by requiring the surface elevation to be continuous

$$[\bar{\zeta}]_-^+ = 0, \tag{2.12}$$

which can be shown to be consistent with continuity in mass and energy flux. Here the limits + and − are to be interpreted as $x \to x_{\mathrm{m}}$ from the right and left, respectively. The other condition arises from integrating (2.9) from x_{m}^- to x_{m}^+, which yields

$$\left[\frac{\partial \bar{\zeta}}{\partial x}\right]_-^+ = -\frac{1}{\rho g h_{\mathrm{m}}}\left[\frac{\partial S_{xx}}{\partial x} + 2\frac{\partial S_{xy}}{\partial y}\right]_-^+. \tag{2.13}$$

This condition renders a kink in $\bar{\zeta}$ possible. However strange this may seem, it is merely a generalization of the usual kink at the break point in the classical calculation of stationary wave set-down/set-up.

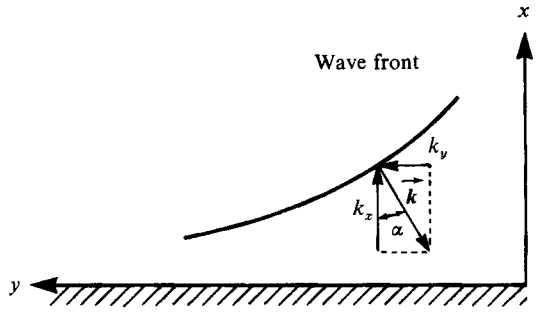

FIGURE 2. Sketch of incident waves. With the choice of coordinate system the wave shown travels in the negative directions. However, with the artifice of choosing $\boldsymbol{k} = (-k_x, -k_y)$ we get positive wavenumber components.

2.2. *Transformation of wave groups in shoaling waters and in surf conditions*

In order to compute the forcing term in the governing equation (2.9) the radiation stress tensor S_{ij} associated with the short waves is needed. To the lowest order of approximation this can be obtained from linear Stokes theory with appropriate modifications in the surf zone. We have (see e.g. Mei 1983, chapter 3, equation 6.42)

$$\frac{1}{\rho g} S_{ij} = \tfrac{1}{2}|A|^2 \left\{ \left(\frac{c_g}{c} - \tfrac{1}{2} \right) \delta_{ij} + \frac{c_g}{c} \frac{k_i k_j}{k^2} \right\}, \tag{2.14}$$

where δ_{ij} is the Kronecker delta and

$$\frac{k_i k_j}{k^2} = \begin{bmatrix} \cos^2\alpha & \frac{1}{2}\sin 2\alpha \\ \frac{1}{2}\sin 2\alpha & \sin^2\alpha \end{bmatrix}, \tag{2.15}$$

α being the local angle of incidence, see figure 2. Here A is a complex amplitude describing the modulation of the short waves, and c_g and c are the group velocity and phase velocity of the short waves, respectively. A is allowed to have a slow variation in time as well as in space, and it is determined by the kinematics and the dynamics of the short waves.

The accuracy of (2.14) is known to decrease towards the break point and in the surf zone it only gives a crude approximation, generally an overestimation, see Svendsen (1984).

2.2.1. *The kinematics*

The most simple case of a modulated wave train is that of a superposition of two monochromatic wave trains of slightly different angular frequencies

$$\omega^{(1)} = \omega_s(1+\epsilon), \quad \omega^{(2)} = \omega_s(1-\epsilon), \tag{2.16}$$

where ω_s is their mean value, and ϵ is a small perturbation parameter. Alternatively, one could have specified a wavenumber perturbation as was done by Mei & Benmoussa (1985), Schäffer & Svendsen (1988) and Liu (1989), but this approach has the disadvantage that the perturbation parameter then has to refer to some fixed depth. Note that the two approaches result in different definitions of ϵ.

The change $\epsilon\omega_s$ in angular frequency corresponds to a change Δk in wavenumber

$$\Delta k = \frac{\Delta k}{\Delta \omega} \epsilon \omega_s \approx \frac{\epsilon \omega_s}{c_g}, \tag{2.17}$$

so that

$$\left.\begin{aligned} k^{(1)} &= k+\epsilon\frac{\omega_s}{c_g} = k\left(1+\epsilon\frac{c}{c_g}\right), \\ k^{(2)} &= k-\epsilon\frac{\omega_s}{c_g} = k\left(1-\epsilon\frac{c}{c_g}\right), \end{aligned}\right\} \tag{2.18}$$

We shall assume that the two waves have the same angle of incidence α_0 at some offshore (horizontal bottom) position. Consequently they will undergo much the same refraction, and we can everywhere use k, α as a mean wavenumber and direction for the short waves.

It will later prove convenient to choose the shore-normal axis positive offshore, see figure 2. The usual consequence of this would be to obtain one (or two) negative wave number component(s) of the wavenumber vector. However, with the artifice of choosing $\boldsymbol{k} = (-k_x, -k_y)$ we conveniently get positive wavenumber components, which we shall also denote k_i, $i = 1, 2$.

Let * denote the complex conjugate of the preceding term, then the elevations of the two wave trains are

$$\left.\begin{aligned} \eta^{(1)} &= \tfrac{1}{2}a^{(1)}\exp\left[\mathrm{i}\left(\int k_i^{(1)}\,\mathrm{d}x_i+\omega^{(1)}t\right)\right]+*, \\ \eta^{(2)} &= \tfrac{1}{2}a^{(2)}\exp\left[\mathrm{i}\left(\int k_i^{(2)}\mathrm{d}x_i+\omega^{(2)}t\right)\right]+*. \end{aligned}\right\} \tag{2.19}$$

Further, k_y is constant on a one-dimensional topography $h = h(x)$ (Snell's law), and the superposition is

$$\begin{aligned} \eta &= \eta^{(1)}+\eta^{(2)} \\ &= \tfrac{1}{2}\exp\left\{\mathrm{i}\left[\int\tfrac{1}{2}(k_x^{(1)}+k_x^{(2)})\,\mathrm{d}x+\tfrac{1}{2}(k_y^{(1)}+k_y^{(2)})\,y+\omega_s t\right]\right\} \\ &\quad\times\{a^{(1)}\exp\left\{\mathrm{i}\left[\int\tfrac{1}{2}(k_x^{(1)}-k_x^{(2)})\,\mathrm{d}x+\tfrac{1}{2}(k_y^{(1)}-k_y^{(2)})\,y+\epsilon\omega_s t\right]\right\} \\ &\quad+a^{(2)}\exp\left\{-\mathrm{i}\left[\int\tfrac{1}{2}(k_x^{(1)}-k_x^{(2)})\,\mathrm{d}x+\tfrac{1}{2}(k_y^{(1)}-k_y^{(2)})\,y+\epsilon\omega_s t\right]\right\}+*. \end{aligned} \tag{2.20}$$

To the leading order in ϵ (i.e. $O(\epsilon^0) = O(1)$) we have

$$\tfrac{1}{2}(k_x^{(1)}+k_x^{(2)}) = k_x, \quad \tfrac{1}{2}(k_y^{(1)}+k_y^{(2)}) = k_y. \tag{2.21}$$

For the difference wavenumbers the leading order is $O(\epsilon)$. Let the subscript 0 refer to the location where the two wavetrains have a common angle of incidence α_0, then we get

$$K_x \equiv k_x^{(1)}-k_x^{(2)} = 2\epsilon\frac{c_0}{c_{g0}}\left[k_x+\frac{k^2}{k_x}\left(\frac{c/c_g}{c_0/c_{g0}}-1\right)\right], \tag{2.22}$$

$$K_y \equiv k_y^{(1)}-k_y^{(2)} = 2\epsilon k_y\frac{c_0}{c_{g0}}, \tag{2.23}$$

see Schäffer (1990) for details. Equation (2.22) compares with (3.9) of Mei &

Benmoussa (1984), and (2.23) is also consistent with their findings. The connection between the present ϵ and their definition (here with the subscript MB) is

$$\epsilon \frac{c_0}{c_{g0}} = \epsilon_{MB}. \tag{2.24}$$

Also, K_x is defined differently:

$$K_x = 2\epsilon_{MB} K_{x,MB}. \tag{2.25}$$

While (2.22) was found directly from the expressions for the two wave trains, Mei & Benmoussa derived their (3.9) from (2.29), see below.

Using (2.21)–(2.23) in (2.20) now yields

$$\eta = \tfrac{1}{2} A \exp\left[\mathrm{i}\left(\int k_x \,\mathrm{d}x + k_y y + \omega_s t\right)\right] + *, \tag{2.26}$$

where

$$A = a^{(1)} \mathrm{e}^{i\theta} + a^{(2)} \mathrm{e}^{-i\theta} \tag{2.27}$$

and

$$\theta = \int \tfrac{1}{2} K_x \,\mathrm{d}x + \tfrac{1}{2} K_y y + \epsilon \omega_s t. \tag{2.28}$$

To the lowest order of approximation the kinematics presented here apply everywhere. This is not true for the dynamics, where the surf zone has to be treated separately.

2.2.2. *The dynamics*

Outside the surf zone energy conservation prescribes to the leading order in short-wave steepness (see e.g. Phillips 1977, §3.6),

$$\frac{\partial |A|^2}{\partial t} - \frac{\partial}{\partial x_i}(c_{g,i} |A|^2) = 0, \tag{2.29}$$

where the minus sign on the second term is a consequence of chosing $\boldsymbol{c}_g = (-c_{gx}, -c_{gy})$ (analogous to $\boldsymbol{k} = (-k_x, -k_y)$) to get positive components of the group velocity vector, see figure 2. Owing to the linear description of the primary waves the two wave trains are described by the usual law for shoaling and refraction,

$$a^2 = \frac{c_{gx,\mathrm{ref}}}{c_{gx}} a_{\mathrm{ref}}^2, \tag{2.30}$$

where a can be either $a^{(1)}$ or $a^{(2)}$ (since according to (2.21) the two wave trains are refracted identically to the lowest order in ϵ), and the subscript ref refers to some reference depth.

We now turn to the modelling of the short-wave amplitude within the surf zone. It is evident that the position of the break point must vary slowly in time owing to the grouping of the incident waves. Let the amplitudes of the two incident wave trains be given by

$$a^{(1)} \equiv a, \quad a^{(2)} \equiv \delta a, \tag{2.31}$$

then δ is a modulation parameter for the short waves. For $\delta = 0$ there is no modulation, and for $\delta = 1$ we have 'genuine' wave groups with nodes in the envelope. In the following we shall assume $\delta \ll 1$ so that only small modulations are treated. This further implies that the variation of the break-point position is small, although not negligible.

The model we shall use for the breaking and shoreward decay of modulated incident waves is a combination of two simple, but basically different, models. We

shall begin with a presentation of each of the two and then show how an interpolation between them yields a more general description.

The first model is obtained by assuming that the short-wave modulation is totally destroyed by the breaking, so that the wave height decay in the surf zone is solely dependent on the local water depth. We shall use the crude approximation of proportionality between the amplitude and the local water depth, which may be written

$$|A|^2 = \gamma_0^2 h^2, \tag{2.32}$$

where γ_0 is a constant often taken as 0.4. Outside the break point we have

$$\begin{aligned} |A|^2 &= a^2(1+\delta^2+2\delta\cos 2\theta) \\ &= a^2[(1+2\delta\cos 2\theta)+O(\delta^2)]. \end{aligned} \tag{2.33}$$

The instantaneous break point $x_b(t)$ is now found as the position where these two amplitudes match. Equating (2.32) with (2.33) yields

$$\begin{aligned} x_b(t) &= \frac{a_b}{\gamma_0 h_x}(1+\delta^2+2\delta\cos 2\theta_b)^{\frac{1}{2}} \\ &= \frac{\bar{a}_b}{\gamma_0 h_x}\left[1+\delta\cos(\phi+K_y y+\omega t)+\left(\frac{1}{a_b}\frac{\mathrm{d}a_b}{\mathrm{d}x}\right)_{x=\bar{x}_b}(x_b-\bar{x}_b)+O(\delta^2)\right], \end{aligned} \tag{2.34}$$

where

$$\omega \equiv 2\epsilon\omega_s = \omega^{(1)}-\omega^{(2)}, \tag{2.35}$$

and h_x is the bottom slope for a linear depth $h = h_x x$. (More generally we can take h_x as the local bottom slope, by which the expressions hold also for non-planar beach profiles provided they are monotonic.) The quantity ϕ is a phase given by

$$\begin{aligned} \phi &\equiv \int_{\text{const.}}^{x_b} K_x \,\mathrm{d}x \\ &= \int_{\text{const.}}^{\bar{x}_b} K_x \,\mathrm{d}x + O(\delta), \end{aligned} \tag{2.36}$$

and it has a weak time dependence of $O(\delta)$, which may be neglected in (2.34), introducing only errors of $O(\delta^2)$. The overbar denotes time-mean over a group period $2\pi/\omega$ so that $\bar{x}_b$ is the mean position of the break point, and the subscript b refers to the break point. Solving (2.34) for x_b, we get

$$x_b(t) = \frac{\bar{a}_b}{\gamma_0 h_x}[1+\mu\delta\cos(\phi+K_y y+\omega t)+O(\delta^2)], \tag{2.37}$$

where

$$\mu \equiv \frac{1}{1+\nu}, \tag{2.38}$$

and

$$\nu \equiv -\left[\frac{x}{a}\frac{\mathrm{d}a}{\mathrm{d}x}\right]_{x=\bar{x}_b}, \tag{2.39}$$

Note that μ is a factor which accounts for the short-wave shoaling and refraction within the region of initial breaking. For normal incidence we have

$$\nu = \left[\frac{1}{2}\frac{h}{c_g}\frac{\mathrm{d}c_g}{\mathrm{d}h}\right]_{h=\bar{h}_b}, \tag{2.40}$$

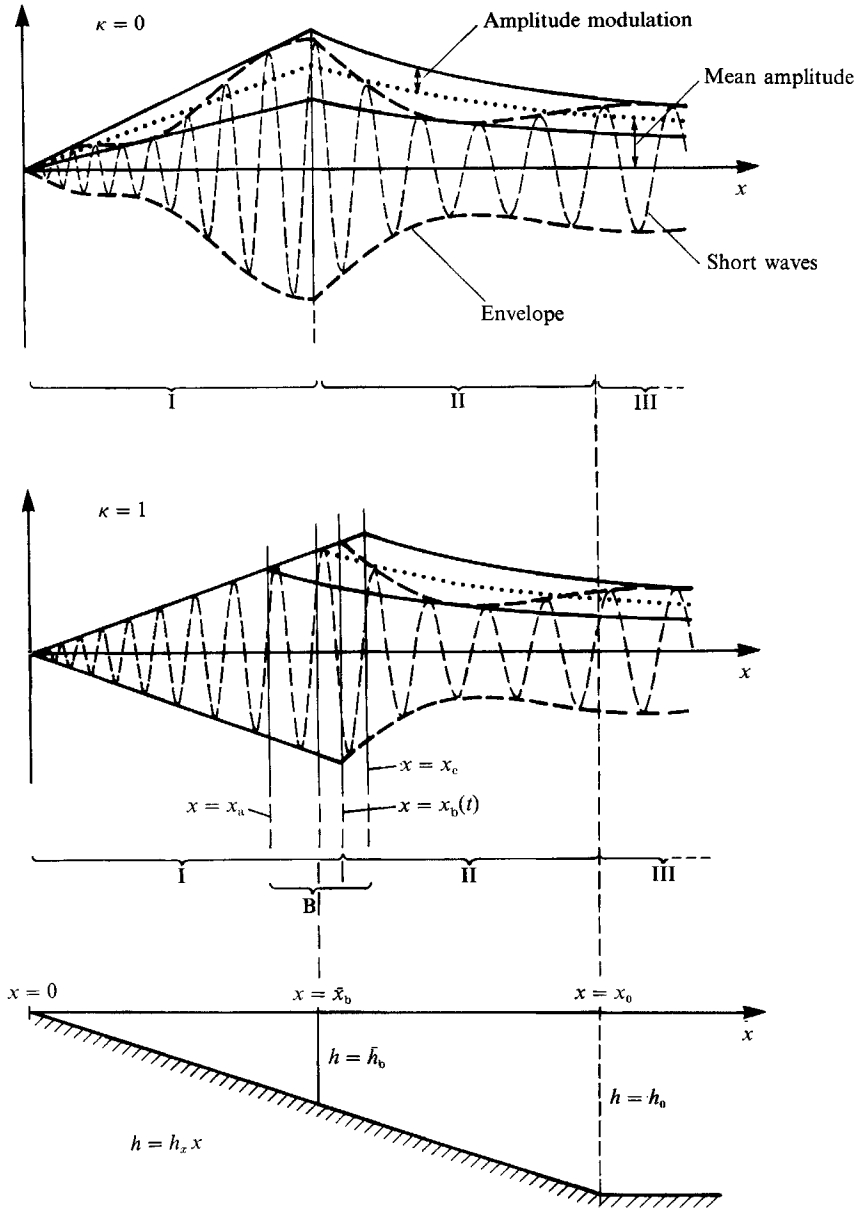

FIGURE 3. Sketch of bottom topography and two examples of short-wave modelling with associated definitions of the regions I, II, B, and III.

so that $0 \lesssim \nu \leqslant \frac{1}{4}$ and thus $\frac{4}{5} \leqslant \mu \lesssim 1$. According to (2.40) ν can in principle be negative, but since this corresponds to breaking at intermediate water depth it will not happen in practice. The deviation of μ from unity was neglected by Schäffer, Jonsson & Svendsen (1990) and Symonds *et al.* (1982).

Equation (2.37) shows that the variation of x_b is essentially harmonic in time with maximum excursions $\mu\delta\bar{x}_b$ away from the mean position, neglecting terms of $O(\delta)^2$.

This model was used by Symonds *et al.* (1982) to study the effect of a time-varying break-point position, and it is illustrated in figure 3, case $\kappa = 1$ (for the definition of

κ, see later). The figure also defines region B as the zone in which initial breaking occurs.

The second model is more simple in that it postulates a fixed break-point position so that x_b is not a function of t. On the other hand, this implies the complication that the short-wave modulation is transmitted into the surf zone. Fixing the break point according to (2.32) without modulation ($\delta = 0$)

$$a_b = \gamma_0 h_b, \tag{2.41}$$

the surf zone amplitude is taken to be

$$|A|^2 = \gamma^2 h^2, \tag{2.42}$$

where γ is chosen so that the amplitude is continuous at the fixed break point, implying that γ is slowly varying with x and t. Equating (2.42) with (2.33) at $x = x_b$ yields

$$\gamma_b^2 = \gamma_0^2(1+\delta^2+2\delta\cos 2\theta_b), \tag{2.43}$$

and we choose to define γ accordingly also inside the break point to get

$$|A|^2 = \gamma_0^2(1+\delta^2+2\delta\cos 2\theta)h^2. \tag{2.44}$$

Thus the amplitude modulation is fully transmitted into the surf zone. This model was used by Schäffer & Svendsen (1988) when studying transformation of incoming bound, long waves, and it is illustrated in figure 3, case $\kappa = 0$.

A hybrid model is now obtained by specifying (see (2.32) and (2.44))

$$|A|^2 = \gamma_0^2[1+(1-\kappa)\,2\delta\cos 2\theta + O(\delta^2)]\,h^2, \tag{2.45}$$

where κ is a parameter at our disposal. Equating this with (2.33) at the break point we obtain

$$x_b(t) = \frac{\bar{a}_b}{\gamma_0 h_x}[1+\mu\kappa\delta\cos(\phi+K_y y+\omega t)+O(\delta^2)]. \tag{2.46}$$

For $\kappa = 0$ the model simplifies to a constant break-point position and a full transmission of grouping into the surf zone. For $\kappa = 1$, the break point oscillates so much that all grouping is destroyed, and the short-wave amplitude is solely a function of the local water depth in the surf zone.

When κ lies in the range $0 < \kappa < 1$, the hybrid model represents an interpolation between these two special cases. The question now is which value should be assigned to κ. Mathematically, we can extrapolate to κ-values out of this range, but is this physically relevant? Clearly $\kappa > 0$, since high waves must break at greater depths than low waves. However, the possibility exists that the higher waves might even break so early that they decay sufficiently to appear as the low waves in the surf zone – whatever grouping was left would be reversed. This would correspond to $\kappa > 1$.

In the absence of experimental results on the break-point variation for incident wave groups we turn to the bulk of data for monochromatic waves collected by Goda (1970). For long group periods ($\epsilon \ll 1$) the breaking will have time to adjust to the local incident wave height, and the measurements for monochromatic waves should suffice.

Figure 4 shows γ_0 as a function of the short-wave steepness in deep water

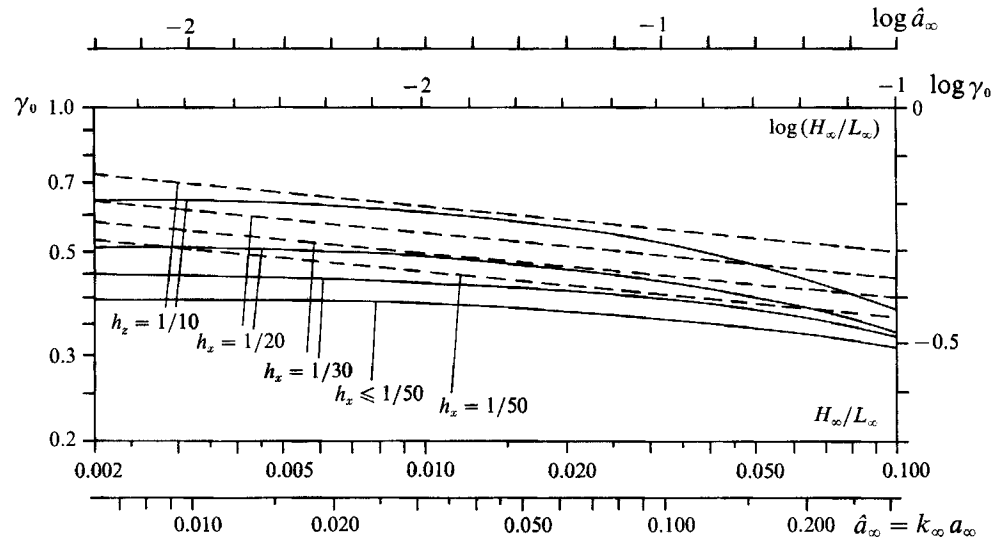

FIGURE 4. Index $\gamma_0 = a_b/h_b$ versus deep-water steepness $\hat{a}_\infty$ for different bottom slopes $h_x = \tan\beta$. Experimental results for monochromatic waves adapted from ——, Goda (1970) and from – – –, Hansen (1990).

$\hat{a}_\infty \equiv (\omega_s^2/g)\,a_\infty$ for different bottom slopes. The full curves were obtained from Goda's figures and the dashed curves are given by

$$\gamma_0 = \frac{1.05}{2}\left[2.87 h_x \left(\frac{\hat{a}_\infty}{\pi}\right)^{-0.45}\right]^{0.2} = 0.72 h_x^{0.2} \hat{a}_\infty^{-0.09}, \tag{2.47}$$

obtained from Hansen's (1990) empirical expressions.

Now the connection between $\gamma_0(\hat{a}_\infty)$ and κ is found from (2.45). The maximum deviation $\Delta(\gamma^2)$ of γ^2 is seen to be

$$\Delta(\gamma^2) = \gamma_0^2(1-\kappa)\,2\delta, \tag{2.48}$$

neglecting terms of order $O(\delta^2)$. The relative change in γ^2 is $\Delta(\gamma^2)/\gamma_0^2 = 2\Delta(\ln\gamma)$ and the relative change in incident short-wave steepness is $\delta = \Delta(\ln\hat{a}_\infty)$. Hence, solving (2.48) for k yields in the limit of infinitesimal variations

$$\kappa = 1 - \frac{\mathrm{d}(\log\gamma_0)}{\mathrm{d}(\log\hat{a}_\infty)}, \tag{2.49}$$

where we have replaced γ with γ_0 in accordance with our use of measurements for unmodulated incident waves. Thus the deviation of k from unity can be found as minus a gradient of the relevant curve in figure 4 measured along the logarithmic axes. These gradients are zero or negative everywhere indicating that we always have $\kappa \geqslant 1$. Hansen's data render κ a universal constant

$$\kappa = 1.09. \tag{2.50}$$

As mentioned before, $\kappa > 1$ represents a reversal of grouping as the short waves pass through the zone of initial breaking. However, as long as κ is close to unity, there is also a substantial reduction in the modulation. For example, $\kappa = 1.1$ only lets 10%

of the original modulation through to the surf zone. The analysis of field data by List (1991) indicates that some wave grouping persists within the surf zone on a natural beach.

3. The energy balance

Before we proceed with the solution of the model described in §2 we shall briefly consider the energy balance in order to gain some physical understanding of the model. A detailed analysis is given in Schäffer (1990).

In the linearized form of the governing equations we have lost the description of the interaction between the incident short waves and the resulting infragravity waves. This is analogous to any other lowest-order perturbation. Here the infragravity waves represent the perturbation of the short-wave climate. The long waves are forced by the short waves which generously feed them with energy without losing any of their own. This is because the short-wave description is independent of the long waves, and our linearized model leaves no room for a feed-back mechanism. This again means that the model breaks down long before the infragravity wave reaches an amplitude comparable to that of the short waves.

In the previous chapter we have used the conservation equations for mass and momentum in which the water motion had already been divided up into a contribution from the infragravity wave (or slowly varying current) and a contribution from the short waves. In order to analyse the energy balance we initially regard the total water motion including both of these.

Equation (3.6.18) of Phillips (1977) states the conservation of total energy can be written as

$$\frac{\partial \mathscr{E}}{\partial t}+\frac{\partial \mathscr{W}_i}{\partial x_i}+\mathscr{E}_{\mathrm{d}}=0 \tag{3.1}$$

where we have included the dissipation per unit area, $\mathscr{E}_{\mathrm{d}}$. Here $\mathscr{E}$ is the total energy density and $\mathscr{W}_i$ is the total energy flux in the x_i-direction ($i = 1, 2$). Dividing the horizontal velocity components into a short-wave component and a (slowly varying) current or long-wave velocity yields

$$\mathscr{E}=E_{\mathrm{c}}+E_{\mathrm{s}}-\tfrac{1}{2}\rho(h+\bar{\zeta})\,U_{\mathrm{s}}^2, \tag{3.2}$$

$$\mathscr{W}_i=\mathscr{W}_{\mathrm{c},i}+\mathscr{W}_{\mathrm{s},i}+U_{\mathrm{c},i}E_{\mathrm{s}}-\tfrac{1}{2}\rho(h+\bar{\zeta})\,U_i U_{\mathrm{s}}^2+U_{\mathrm{c},j}S_{ij}. \tag{3.3}$$

Here E is an energy density, and W is an energy flux, and the subscripts c and s refer to the current (or long waves) and the short waves, respectively. Furthermore, U and U_{s} are the lengths of the horizontal velocity vectors with the components U_i and $U_{\mathrm{s},i}$, respectively, given by (2.4). Note that E_{c} and $W_{\mathrm{c},i}$ are defined using U_i rather than $U_{\mathrm{c},i}$:

$$E_{\mathrm{c}}=\tfrac{1}{2}\rho(h+\bar{\zeta})\,U^2+\tfrac{1}{2}\rho g\bar{\zeta}^2, \tag{3.4}$$

$$W_{\mathrm{c},i}=U_i(h+\bar{\zeta})(\tfrac{1}{2}\rho U^2+\rho g\bar{\zeta}). \tag{3.5}$$

This is a convenient choice, since it is U_i that appears in the conservation equations for mass and momentum. (The opposite choice would change the interpretation of (3.2) and (3.3) as to how large the contributions to the total quantities ($\mathscr{E}$, $\mathscr{W}_i$) were, owing to the current (E_{c}, $W_{\mathrm{c},i}$) and the interaction terms, respectively.)

Equation (3.1) can be split up into two new equations, one for the short waves and one for the total current, U_i (the current excluding the return flow due to the mass transport of the short waves). Subtracting $\rho(h+\bar{\zeta})\,U_i$ times the momentum equation

(2.6) and $(\rho g\overline{\zeta}+\frac{1}{2}\rho U^2)$ times the equation of mass conservation (2.5)† from the total energy equation (3.1) we obtain the energy equation for the short waves

$$\frac{\partial}{\partial t}\{E_s-\tfrac{1}{2}\rho(h+\overline{\zeta})\,U_s^2\}+\frac{\partial}{\partial x_i}\{U_{c,i}E_s+W_{s,i}-\tfrac{1}{2}\rho(h+\overline{\zeta})\,U_i\,U_s^2\}$$
$$+S_{ij}\frac{\partial U_{c,i}}{\partial x_i}-U_{s,j}\frac{\partial S_{ij}}{\partial x_i}+E_d=0, \quad (3.6)$$

where E_d is the short-wave dissipation. The last term but one is missing in equation (3.6.19) of Phillips (1977) where it should have been included. Usually this term is small (i.e. for $|U_c| \gg |U_s|$), but when U_c and U_s are of the same order of magnitude, the term is comparable to the preceding one. This is, for example, the case if U_c corresponds to a long, forced wave at depths that are large relative to the short waves.

Subtracting the short-wave energy equation from the total energy equation yields the energy equation for the total current. Equivalently this equation can be obtained by adding $\rho(h+\overline{\zeta})\,U_i$ times the momentum equation (2.6) to $(\rho g\overline{\zeta}+\frac{1}{2}\rho U^2)$ times the equation of mass conservation (2.5). We get

$$\frac{\partial E_c}{\partial t}+\frac{\partial W_{c,i}}{\partial x_i}+U_i\frac{\partial S_{ij}}{\partial x_j}=0. \quad (3.7)$$

This equation is equivalent to (3.6.22) of Phillips (1977) except for the last term, where he has $U_{c,i}$ instead of U_i. Note that (3.7) becomes an identity for zero total current $U_i \equiv 0$, whereas Phillips (3.6.22) becomes unbalanced. The last term is (3.7) is the work done on the long waves by the short waves.

In the applications in §4 we shall compute the time mean over a group period of the energy flux for the long waves. A spatial variation of this quantity illustrates how the long waves can change from having the character of a standing wave at the coastline to being of progressive nature further offshore. Thus, the mean long-wave energy flux will be helpful when interpreting the numerical results for the infragravity wave surface elevation.

4. Two-dimensional infragravity wave motion – normally incident wave groups

We now turn to the case of normally incident groups of short waves. Assuming a one-dimensional topography $h = h(x)$ the radiation stress has no variation in the longshore direction, and hence the short-wave forcing will result in two-dimensional infragravity waves. Of course three-dimensional free waves can still exist, but they cannot originate from the forcing mechanisms considered in the present work. We shall only consider a plane sloping beach connected with an offshore shelf, see figure 3.

4.1. *Governing equations*

In the one-dimensional case the long-wave equation (2.9) reduces to

$$\frac{\partial}{\partial x}\left(gh\frac{\partial\overline{\zeta}}{\partial x}\right)-\frac{\partial^2\overline{\zeta}}{\partial t^2}=-\frac{1}{\rho}\frac{\partial^2 S_{xx}}{\partial x^2}, \quad (4.1)$$

† The combinations $\rho(h+\overline{\zeta})\,U_i\times(2.26)+(\rho g\overline{\zeta}+\frac{1}{2}\rho U^2)\times(2.5)$ can be substituted by $\rho U_i\times(2.2)+(\rho g\overline{\zeta}-\frac{1}{2}\rho U^2)\times(2.5)$ as used by Phillips (1977).

where from (2.14)

$$\frac{1}{\rho g} S_{xx} = \tfrac{1}{2}|A|^2 \left\{ \frac{2c_g}{c} - \tfrac{1}{2} \right\}. \tag{4.2}$$

Neglecting terms of $O(\delta^2)$ we have from (2.45) and (2.33)

$$|A|^2 = \begin{cases} \gamma_0^2 h^2 [1 + (1-\kappa) 2\delta \cos 2\theta] & (x \leqslant x_b(t)), \\ a^2 (1 + 2\delta \cos 2\theta) & (x \geqslant x_b(t)), \end{cases} \tag{4.3}$$

where from (2.46) the position of initial wave breaking is

$$x_b(t) = \frac{\bar{a}_b}{\gamma_0 h_x} (1 + \mu\kappa\delta \cos \omega t), \tag{4.4}$$

choosing $\phi = 0$. Consistent with this choice we have from (2.22), (2.28), (2.35) and (2.36)

$$2\theta = \int_{\bar{x}_b}^{x} \frac{\omega}{c_g} \mathrm{d}x + \omega t, \tag{4.5}$$

and from (2.30)

$$a^2 = \frac{c_{g\infty}}{c_g} a_\infty^2 \quad (x \geqslant x_b(t)), \tag{4.6}$$

choosing deep water as reference.

4.2. *Theoretical infragravity wave solution*

4.2.1. *General solution*

Restricting ourselves to study only infragravity wave phenomena that are periodic in time we introduce the Fourier expansions of the elevation of mean water surface $\bar{\zeta}$ and the radiation stress S_{xx}

$$\bar{\zeta} = \sum_{n=0}^{\infty} \tfrac{1}{2}(\xi_n(x) \, \mathrm{e}^{\mathrm{i}n\omega t} + *), \tag{4.7}$$

$$S_x = \sum_{n=0}^{\infty} \tfrac{1}{2}(S_n(x) \, \mathrm{e}^{\mathrm{i}n\omega t} + *), \tag{4.8}$$

where *, as before, denotes the complex conjugate of the preceding term. Now (4.1) transforms into the ordinary differential equations

$$\frac{\mathrm{d}}{\mathrm{d}x}\left(gh \frac{\mathrm{d}\xi_n}{\mathrm{d}x} \right) + (n\omega)^2 \xi_n = -\frac{1}{\rho} \frac{\mathrm{d}^2 S_n}{\mathrm{d}x^2} \quad (n = 0, 1, 2, \dots). \tag{4.9}$$

The case $n = 0$, for which (4.9) can be integrated directly, determines the stationary set-down or set-up, and it will not be pursued further. The rest of (4.9) governs the infragravity wave motion which we shall concentrate on in the following.

By the method of variation of parameters, the solution to (4.9) may be expressed as

$$\xi_n = -\xi_n^{(1)} \left(-\alpha_n + \int_{x_l}^{x} \frac{\xi_n^{(2)} q_n}{W_n} \mathrm{d}x \right) + \xi_n^{(2)} \left(\beta_n + \int_{x_l}^{x} \frac{\xi_n^{(1)} q_n}{W_n} \mathrm{d}x \right) \quad (n = 1, 2, 3, \dots), \tag{4.10}$$

where $\xi_n^{(1)}$ and $\xi_n^{(2)}$ are linearly independent homogeneous solutions (free waves), W_n is their Wronskian, q_n is the right-hand side of the normalized equation (4.9)

$$q_n = -\frac{1}{\rho g h}\frac{\mathrm{d}^2 S_n}{\mathrm{d}x^2} \quad (n = 1, 2, 3, \dots), \tag{4.11}$$

and α_n and β_n are arbitrary complex constants. Any lower limit of integration x_l in (4.10) can be chosen.

So far all derivations are valid for an arbitrary one-dimensional depth variation $h = h(x)$ with the restrictions that it should be 'sufficiently' smooth and have a monotonic variation within and near the surf zone. Also the depth must everywhere be small compared with the lengthscale of the infragravity waves. In the following, we shall confine ourselves to a plane sloping beach $h = h_x x$ connected to a shelf $h = h_0$ at some distance seawards of the break point. Figure 3 shows a cross-section with definitions of four regions I, II, B, and III. Region I is the surf zone taken as $0 \leqslant x \leqslant x_b(t)$, where $x_b(t)$ is the variable position of the break point, region II is the shoaling zone $x_b(t) \leqslant x \leqslant x_0 = h_0/h_x$, and region III is the shelf zone $x \geqslant x_0 - $ a constant depth zone inferred to enable us to specify a seaward boundary condition for the solutions in regions I and II. Region III also serves the purpose of limiting the water depth to keep it small for the infragravity wave motion (although it may well be deep water for the short waves). Region B is the zone of initial breaking given by $x_a \leqslant x \leqslant x_c$, see figure 3, case $\kappa = 1$. Thus region B overlaps regions I and II.

In regions I and II we have $h = h_x x$, and choosing a complex representation the free wave solutions (homogeneous solutions) to (4.9) are given by the Hankel functions of the first and second kind of order zero ($n = 1, 2, 3, \dots$)

$$\left.\begin{aligned} \xi_n^{(1)} &= H_0^{(1)}(ny') = J_0(ny') + \mathrm{i}Y_0(ny'), \\ \xi_n^{(2)} &= H_0^{(2)}(ny') = J_0(ny') - \mathrm{i}Y_0(ny'), \end{aligned}\right\} \tag{4.12}$$

where J_0 and Y_0 are zeroth order Bessel functions of first and second kind, and

$$y' \equiv \frac{2\omega}{gh_x}(gh)^{\frac{1}{2}}, \quad \frac{\mathrm{d}y'}{\mathrm{d}x} = \frac{\omega}{(gh)^{\frac{1}{2}}}. \tag{4.13}$$

Their Wronskian (see e.g. 9.1.17, Abramowitz & Stegun 1972) with respect to x is

$$W_n\{H_0^{(1)}(ny'(x)),\, H_0^{(2)}(ny'(x))\} = -\frac{4\mathrm{i}}{\pi n y'}\frac{\mathrm{d}}{\mathrm{d}x}(ny') = -\frac{2\mathrm{i}}{\pi x}, \tag{4.14}$$

and we get

$$\frac{q_n}{W_n} = -\frac{\mathrm{i}\pi}{2\rho g h_x}\frac{\mathrm{d}^2 S_n}{\mathrm{d}x^2}, \tag{4.15}$$

after which (4.10) yields

$$\begin{aligned} \xi_n^{(J)} = {} & \frac{\mathrm{i}\pi}{2\rho g h_x} H_0^{(1)}(ny')\left(-\alpha_n^{(J)} + \int_{x_l}^{x} H_0^{(2)}(ny')\frac{\mathrm{d}^2 S_n^{(J)}}{\mathrm{d}x^2}\mathrm{d}x\right) \\ & - \frac{\mathrm{i}\pi}{2\rho g h_x} H_0^{(2)}(ny')\left(\beta_n^{(J)} + \int_{x_l}^{x} H_0^{(1)}(ny')\frac{\mathrm{d}^2 S_n^{(J)}}{\mathrm{d}x^2}\mathrm{d}x\right) \quad (J = \mathrm{I}, \mathrm{II}, \quad n = 1, 2, 3, \dots), \end{aligned} \tag{4.16}$$

redefining the constants.

On the *shelf* the solution to (4.9) is easily verified to be

$$\xi_n^{(\mathrm{III})} = \alpha_n^{(\mathrm{III})} \exp\left(\mathrm{i}\frac{n\omega}{(gh_0)^{\frac{1}{2}}}x\right) + \beta_n^{(\mathrm{III})} \exp\left(-\mathrm{i}\frac{n\omega}{(gh_0)^{\frac{1}{2}}}x\right) + \begin{cases} -\dfrac{1}{\rho g h_0 - c_{go}^2} S_1^{(\mathrm{III})} & (n=1), \\ 0 & (n=2,3,4,\ldots), \end{cases} \tag{4.17}$$

using (4.20) and (4.21) below. Here the particular solution (last term) is the bound, long wave found by Longuet-Higgins & Stewart (1962, 1964).

The assumption of wave groups made up from only two wave components reduces the radiation stress (4.8) to

$$S_x^{(J)} = S_0^{(J)} + \tfrac{1}{2}(S_1^{(J)} \mathrm{e}^{\mathrm{i}\omega t} + *) \quad (J = \mathrm{I}, \mathrm{II}, \mathrm{III}), \tag{4.18}$$

where J refers to the three regions. This is consistent with (4.2), (4.3) and (4.5), and we have

$$S_0 = \tfrac{1}{2}\rho g \left\{\frac{2c_g}{c} - \frac{1}{2}\right\} \begin{cases} \gamma_0^2 h^2 & (x \leqslant x_b(t)), \\ a^2 & (x \geqslant x_b(t)), \end{cases} \tag{4.19}$$

and

$$S_1 = \tfrac{1}{2}\rho g \left\{\frac{2c_g}{c} - \frac{1}{2}\right\} \begin{cases} \gamma_0^2 h^2 (1-\kappa)\, 2\delta \exp\left(\mathrm{i}\displaystyle\int_{\bar{x}_b}^{x} \frac{\omega}{c_g}\mathrm{d}x\right) & (x \leqslant x_b(t)), \\ a^2 2\delta \exp\left(\mathrm{i}\displaystyle\int_{\bar{x}_b}^{x} \frac{\omega}{c_g}\mathrm{d}x\right) & (x \geqslant x_b(t)), \end{cases} \tag{4.20}$$

by which S_{xx} in the three regions may be written

$$S_x = \begin{cases} S_0^{(\mathrm{I})}(1 + 2\delta(1-\kappa)\cos 2\theta) & (x \leqslant x_b(t)), \\ S_0^{(\mathrm{II})}(1 + 2\delta \cos 2\theta) & (x_b(t) \leqslant x \leqslant x_0), \\ S_0^{(\mathrm{III})}(1 + 2\delta \cos 2\theta) & (x_0 \leqslant x). \end{cases} \tag{4.21}$$

Note that S_{xx} is continuous at $x_b(t)$ (and elsewhere), since this (through continuity in $|A|^2$) was the criterion when the variation of $x_b(t)$ was found, see the end of §2.2.2.

Away from region B the Fourier coefficients of S_{xx} are given by (4.19) and (4.20), and in each region the solution for the elevation can be found from (4.10). In region B, however, (4.19) and (4.20) are *not* the Fourier coefficients of the radiation stress, since they have an implicit time-dependence given through the variable break point position. This feature is essential for the impact of a time-varying break point position.

4.2.2. *The effect of oscillations of the break point position*

This subsection takes up the rather special circumstances in the zone of initial breaking, region B.

Consistent with the chosen form of the Fourier expansion (4.8) we have

$$S_0 = \frac{1}{2\pi}\int_{-\pi}^{\pi} S_{xx}\, \mathrm{d}(\omega t), \tag{4.22}$$

and

$$S_n = \frac{1}{\pi}\int_{-\pi}^{\pi} S_x \, \mathrm{e}^{-\mathrm{i}n\omega t}\, \mathrm{d}(\omega t) \quad (n = 1, 2, 3, \dots). \tag{4.23}$$

Again, since the goal is to study the low-frequency motion and not the stationary set-down and set-up, S_0 is irrelevant. From (4.4) it is seen that the extent of region B is $O(\delta)$ by which 2θ from (4.5) may be approximated by ωt within an error of $O(\delta)$. Introducing this in (4.21) the error becomes $O(\delta^2)$, which we accept. This approximation makes S_{xx} an even function of time, and we get

$$S_n^{(\mathrm{B})} = \frac{2}{\pi}\left(\int_0^{\tau} S_{xx}^{(\mathrm{I})} \cos(n\omega t)\, \mathrm{d}(\omega t) + \int_{\tau}^{\pi} S_{xx}^{(\mathrm{II})} \cos(n\omega t)\, \mathrm{d}(\omega t) \right) \quad (n = 1, 2, 3, \dots) \tag{4.24}$$

where $0 \leqslant t \leqslant \tau/\omega$ and $\tau/\omega \leqslant t \leqslant \pi$ are the time intervals of which we have surf conditions and shoaling conditions, respectively, for a point in region B. Since these intervals vary from point to point then $\tau = \tau(x)$. From (4.4) we have

$$\tau(x) = \arccos\left(\frac{x_{\mathrm{b}}/\bar{x}_{\mathrm{b}} - 1}{\mu\kappa\delta} \right) \quad (x_{\mathrm{a}} \leqslant x \leqslant x_{\mathrm{c}}). \tag{4.25}$$

Note that both (4.4) and (4.25) are expressions for the curve in the (x, t)-plane on which breaking occurs; in (4.4) the point of breaking is given with t as the independent variable, while in (4.25) the time of breaking is given with x as the independent variable. Differentiation of (4.24) yields

$$\frac{\mathrm{d}S_n^{(\mathrm{B})}}{\mathrm{d}x} = \frac{2}{\pi}\left(\int_0^{\tau} \frac{\mathrm{d}S_{xx}^{(\mathrm{I})}}{\mathrm{d}x} \cos(n\omega t)\, \mathrm{d}(\omega t) + \int_{\tau}^{\pi} \frac{\mathrm{d}S_{xx}^{(\mathrm{II})}}{\mathrm{d}x} \cos(n\omega t)\, \mathrm{d}(\omega t) \right) \quad (n = 1, 2, 3, \dots), \tag{4.26}$$

since the terms arising from the variable limits of the two integrals cancel each other, because S_{xx} is continuous at the instantaneous break point.

Replacing 2θ by ωt in (4.21) (see the comment above) it follows that neglecting $O(\delta^2)$ we get

$$\begin{aligned} \frac{\mathrm{d}S_n^{(\mathrm{B})}}{\mathrm{d}x} &= \frac{2}{\pi}\int_0^{\pi} \frac{\mathrm{d}S_0^{(\mathrm{I})}}{\mathrm{d}x} [1 + 2\delta(1-\kappa)\cos\omega t] \cos(n\omega t)\, \mathrm{d}(\omega t) \\ &\quad + \frac{2}{\pi}\int_{\tau}^{\pi} \frac{\mathrm{d}S_0^{(\mathrm{II})}}{\mathrm{d}x} (1 + 2\delta\cos\omega t) \cos(n\omega t)\, \mathrm{d}(\omega t) \quad (n = 1, 2, 3, \dots). \end{aligned} \tag{4.27}$$

Further

$$\begin{aligned} \frac{\mathrm{d}S_n^{(\mathrm{B})}}{\mathrm{d}x} &= \frac{2}{\pi}\frac{\mathrm{d}S_0^{(\mathrm{I})}}{\mathrm{d}x}\left\{ \frac{\sin(n\tau)}{n} + 2\delta(1-\kappa) f_n(\tau) \right\} \\ &\quad - \frac{2}{\pi}\frac{\mathrm{d}S_0^{(\mathrm{II})}}{\mathrm{d}x}\left\{ \frac{\sin(n\tau)}{n} + 2\delta g_n(\tau) \right\} \\ &= \frac{2}{n\pi}\left(\frac{\mathrm{d}S_0^{(\mathrm{I})}}{\mathrm{d}x} - \frac{\mathrm{d}S_0^{(\mathrm{II})}}{\mathrm{d}x} \right) \sin(n\tau) + O(\delta) \quad (n = 1, 2, 3, \dots), \end{aligned} \tag{4.28}$$

where

$$f_n(\tau) \equiv \begin{cases} \frac{1}{2}\tau + \frac{1}{4}\sin 2\tau & (n = 1), \\ \dfrac{\sin((n-1)\tau)}{2(n-1)} + \dfrac{\sin((n+)\tau)}{2(n+1)} & (n = 2, 3, 4, \dots), \end{cases} \tag{4.29}$$

and

$$g_n(\tau) \equiv \begin{cases} f_1(\tau) - \frac{1}{2}\pi & (n = 1), \\ f_n(\tau) & (n = 2, 3, 4, \ldots). \end{cases} \tag{4.30}$$

Here it is only important to know that $f_n(\tau)$ and $g_n(\tau)$ are $O(1)$ in δ, and their explicit appearance is given for later use. At the extreme positions of the break point we have from (4.25)

$$\tau(x_a) = \pi, \quad \tau(x_c) = 0, \tag{4.31}$$

by which (4.28) gives

$$\frac{\mathrm{d}S_n^{(B)}}{\mathrm{d}x}\bigg|_{x=x_a} = \begin{cases} 2\delta(1-\kappa)\dfrac{\mathrm{d}S_0^{(I)}}{\mathrm{d}x}\bigg|_{x=x_a} & (n = 1), \\ 0 & (n = 2, 3, 4, \ldots), \end{cases} \tag{4.32}$$

and

$$\frac{\mathrm{d}S_n^{(B)}}{\mathrm{d}x}\bigg|_{x=x_c} = \begin{cases} 2\delta\dfrac{\mathrm{d}S_0^{(II)}}{\mathrm{d}x}\bigg|_{x=x_c} & (n = 1), \\ 0 & (n = 2, 3, 4, \ldots). \end{cases} \tag{4.33}$$

Returning to the expression for the elevation (4.10) we can write a particular solution in region B as

$$\begin{aligned} \xi_n^{(B)} = {} & \frac{\pi}{\rho g h_x} J_0(ny') \int_{x_a}^{x} Y_0(ny') \frac{\mathrm{d}^2 S_n^{(B)}}{\mathrm{d}x^2}\,\mathrm{d}x \\ & - \frac{\pi}{\rho g h_x} Y_0(ny') \int_{x_a}^{x} J_0(ny') \frac{\mathrm{d}^2 S_n^{(B)}}{\mathrm{d}x^2}\,\mathrm{d}x, \end{aligned} \tag{4.34}$$

where we have used the real representation

$$\xi_n^{(1)} = J_0(ny'), \quad \xi_n^{(2)} = Y_0(ny'), \tag{4.35}$$

with the corresponding Wronskian (see e.g. Abramowitz & Stegun 1972, equation 9.1.16)

$$W_n\{J_0(ny'(x)), Y_0(ny'(x))\} = \frac{2}{\pi n y'} \frac{\mathrm{d}(ny')}{\mathrm{d}x} = \frac{1}{\pi x}, \tag{4.36}$$

and $n = 1, 2, 3, \ldots$ is understood. Integration by parts yields

$$\begin{aligned} \xi_n^{(B)} = {} & \frac{\pi}{\rho g h_x} J_0(ny') \left(\left[Y_0(ny') \frac{\mathrm{d}S_n^{(B)}}{\mathrm{d}x} \right]_{x_a}^{x} + \int_{x_a}^{x} Y_1(ny') \frac{\mathrm{d}(ny')}{\mathrm{d}x} \frac{\mathrm{d}S_n^{(B)}}{\mathrm{d}x}\,\mathrm{d}x \right), \\ & - \frac{\pi}{\rho g h_x} Y_0(ny') \left(\left[J_0(ny') \frac{\mathrm{d}S_n^{(B)}}{\mathrm{d}x} \right]_{x_a}^{x} + \int_{x_a}^{x} J_1(ny') \frac{\mathrm{d}(ny')}{\mathrm{d}x} \frac{\mathrm{d}S_n^{(B)}}{\mathrm{d}x}\,\mathrm{d}x \right), \end{aligned} \tag{4.37}$$

using the identities

$$\frac{\mathrm{d}}{\mathrm{d}z}[J_0(z)] = -J_1(z), \quad \frac{\mathrm{d}}{\mathrm{d}z}[Y_0(z)] = -Y_1(z). \tag{4.38}$$

Here the contributions from the upper variable endpoints cancel each other. Further we can approximate $J_0(ny')$ by $J_0(ny'_a)$ (and likewise for $Y_0(ny')$) introducing only errors of $O(\delta)$, which multiplied by $\mathrm{d}S_n^{(B)}/\mathrm{d}x$ taken at $x = x_a$ (see (4.32)) become $O(\delta^2)$,

which we accept. Hereby also the contributions from the lower endpoints cancel and we are left with

$$\xi_n^{(\mathrm{B})} = \frac{\pi}{\rho g h_x} J_0(ny') \int_{x_a}^{x} Y_1(ny') \frac{\mathrm{d}(ny')}{\mathrm{d}x} \frac{\mathrm{d}S_n^{(\mathrm{B})}}{\mathrm{d}x} \mathrm{d}x$$

$$- \frac{\pi}{\rho g h_x} Y_0(ny') \int_{x_a}^{x} J_1(ny') \frac{\mathrm{d}(ny')}{\mathrm{d}x} \frac{\mathrm{d}S_n^{(\mathrm{B})}}{\mathrm{d}x} \mathrm{d}x. \tag{4.39}$$

Now all variables except τ are slowly varying in region B, and within errors of $O(\delta)$ (giving errors of $O(\delta^2)$ on $\xi_n^{(\mathrm{B})}$) they can be approximated by their values at the mean break-point position. Using (4.28) this results in

$$\xi_n^{(\mathrm{B})} = -\left[\frac{1}{\rho g h_x x}\left(\frac{\mathrm{d}S_0^{(\mathrm{I})}}{\mathrm{d}x} - \frac{\mathrm{d}S_0^{(\mathrm{II})}}{\mathrm{d}x}\right)\right]_{x=\bar{x}_b} \int_{x_a}^{x} \frac{2}{n\pi} \sin(n\tau)\, \mathrm{d}x, \tag{4.40}$$

where we have also used (4.36) and (4.38). The integral is evaluated using (4.25) and we have

$$\int_{x_a}^{x} \frac{2}{n\pi} \sin(n\tau)\, \mathrm{d}x = -\bar{x}_b \mu\kappa\delta \int_{\pi}^{\tau} \frac{2}{n\pi} \sin(n\tau) \sin\tau\, \mathrm{d}\tau$$

$$= \begin{cases} -\bar{x}_b \mu\kappa\delta \dfrac{2}{\pi}\left(\dfrac{\tau-\pi}{2} - \dfrac{\sin 2\tau}{4}\right) & (n=1), \\ -\bar{x}_b \mu\kappa\delta \dfrac{2}{n\pi}\left(\dfrac{\sin[(n-1)\tau]}{2(n-1)} - \dfrac{\sin[(n+1)\tau]}{2(n+1)}\right) & (n=2,3,4,\ldots). \end{cases} \tag{4.41}$$

Together with (4.40) this gives the variation of a particular solution in region B. Being uninterested in the details of the solution in this small region, we shall concentrate on the overall significance of the above result. For $x = x_c$ (4.41) reduces to

$$\int_{x_a}^{x_c} \frac{2}{n\pi} \sin(n\tau)\, \mathrm{d}x = \begin{cases} \bar{x}_b \mu\kappa\delta & (n=1), \\ 0 & (n=2,3,4,\ldots), \end{cases} \tag{4.42}$$

by which the 'jump' in the elevation over region B can be written (see (4.40))

$$\left.\begin{aligned} [\xi_1]_-^+ &= \frac{\mu\kappa\delta}{\rho g h_x}\left[\frac{\mathrm{d}S_0}{\mathrm{d}x}\right]_-^+ \\ [\xi_n]_-^+ &= 0 \quad (n=2,3,4,\ldots), \end{aligned}\right\} \quad (x=\bar{x}_b), \tag{4.43}$$

where we have replaced the endpoints of region B with $\bar{x}_b$ consistent with earlier approximations. Now S_0 is formally taken from the two cases in (4.19) as valid for a vanishing extent of region B. Note that the right-hand side of (4.43*a*) is always negative ($\kappa > 0$).

Thus we have arrived at the important result that to the leading order in δ there is no net forcing of higher harmonics in region B, while the forcing of the fundamental is $O(\delta)$. This is also true away from region B, since we have that S_1 (which is responsible for the forcing of ξ_1) is $O(\delta)$ here, while $S_n = 0$ for $n = 2, 3, 4\ldots$. Altogether this means that the influence of the overall short-wave forcing is of the same order of magnitude as the influence of the time-varying break-point position.

Physically, we may explain the importance of the latter as a result of oscillations in the starting point of the set-up, affecting the whole surf zone and not only region B. Had $S_n^{(B)}$ only been a weighted mean of $S_n^{(I)}$ and $S_n^{(II)}$, it would have been of no significance.

We now turn to the gradient of the surface elevation to investigate whether the elevation has a 'kink' over region B as well as the jump derived above. Differentiation of (4.34) followed by integration by parts yields

$$\frac{\mathrm{d}\xi_n^{(B)}}{\mathrm{d}x} = -\frac{\pi}{\rho g h_x}\frac{\mathrm{d}(ny')}{\mathrm{d}x}J_1(ny')\left(\left[Y_0(ny')\frac{\mathrm{d}S_n^{(B)}}{\mathrm{d}x}\right]_{x_a}^{x} + \int_{x_a}^{x} Y_1(ny')\frac{\mathrm{d}(ny')}{\mathrm{d}x}\frac{\mathrm{d}S_n^{(B)}}{\mathrm{d}x}\mathrm{d}x\right)$$
$$+\frac{\pi}{\rho g h_x}\frac{\mathrm{d}(ny')}{\mathrm{d}x}Y_1(ny')\left(\left[J_0(ny')\frac{\mathrm{d}S_n^{(B)}}{\mathrm{d}x}\right]_{x_a}^{x} + \int_{x_a}^{x} J_1(ny')\frac{\mathrm{d}(ny')}{\mathrm{d}x}\frac{\mathrm{d}S_n^{(B)}}{\mathrm{d}x}\mathrm{d}x\right). \tag{4.44}$$

This expression is analogous to (4.37), only now the integrals cancel within the accuracy of $O(\delta)$, and the remainder can consistently be approximated by

$$\frac{\mathrm{d}\xi_n^{(B)}}{\mathrm{d}x} = -\frac{\pi}{\rho g h_x}\frac{\mathrm{d}(ny')}{\mathrm{d}x}[J_1(ny')Y_0(ny') - J_0(ny')Y_1(ny')]\left[\frac{\mathrm{d}S_n^{(B)}}{\mathrm{d}x}\right]_{x_a}^{x}. \tag{4.45}$$

Note that here we could not have approximated the arguments of the Bessel functions by their values at any other position in region B as we did above, since $\mathrm{d}S_n^{(B)}/\mathrm{d}x$ is generally $O(1)$ (except at $x = x_a$ and $x = x_c$, see (4.28)), by which the total error of the right-hand side of (4.45) would have been $O(\delta)$ and not $O(\delta^2)$.

Using (4.36) and (4.38) now yields

$$\frac{\mathrm{d}\xi_n^{(B)}}{\mathrm{d}x} = -\frac{1}{\rho g h_x x}\left[\frac{\mathrm{d}S_n^{(B)}}{\mathrm{d}x}\right]_{x_a}^{x}. \tag{4.46}$$

Equivalent to (4.43) we are mainly interested in the kink in the elevation over region B. This may be written

$$\left.\begin{aligned}\left[\frac{\mathrm{d}\xi_1}{\mathrm{d}x}\right]_-^+ &= -\frac{1}{\rho g h_x \bar{x}_b}\left[\frac{\mathrm{d}S_1}{\mathrm{d}x}\right]_-^+ \\ \left[\frac{\mathrm{d}\xi_1}{\mathrm{d}x}\right]_-^+ &= 0 \quad (n = 2, 3, 4, \ldots),\end{aligned}\right\} \quad (x = \bar{x}_b), \tag{4.47}$$

where S_1 is now formally taken from the two cases in (4.20) as valid for a vanishing extent of region B.

This means that there is a kink in the elevation of the fundamental, but no kink in the higher harmonics, which do not exist anyway. Comparing this result with the matching conditions, we see that (4.47) satisfies (2.13). However, (4.43) replaces (2.12).

Thus the important conclusion of this subsection is that we can incorporate the effect of oscillations of the break-point position in the overall solution for the surface elevation by simply ignoring the presence of region B and replacing the continuity condition (2.12) by the discontinuity condition (4.43).

In this way the large change in elevation over region B is concentrated in a discontinuity at the mean break-point position, locally losing the details of the

solution. However, we have made sure that globally the solution is not affected by this simplification.

4.2.3. *Determination of integration constants*

There are two complex constants in three regions to be determined, and we have two boundary conditions and four matching conditions providing the necessary six complex equations.

The seaward boundary condition (see §2.1.2) is that of no incoming free, long waves, which requires $\alpha_1^{(\mathrm{III})} = 0$. In region I we take $x_l = 0$ as the lower limit of integration in (4.16), by which the particular part of the solution vanishes at the shoreline. Now the finite-amplitude reflection condition (2.13) yields $\alpha_1^{(\mathrm{I})} = \beta_1^{(\mathrm{I})}$, by which the solution becomes proportional to $J_0(y')$ in the shoreline limit.

The matching conditions are given by (2.12), (2.13) and (4.43).

4.2.4. *Horizontal particle velocity and mean energy flux*

Introducing the Fourier expansion of the linearized horizontal long-wave particle velocity

$$U = \sum_{n=0}^{\infty} \tfrac{1}{2}(U_n(x)\,\mathrm{e}^{\mathrm{i}n\omega t} + *), \tag{4.48}$$

we get from the equation of conservation of momentum (2.8)

$$U_n = \frac{\mathrm{i}}{n\omega}\left(g\frac{\mathrm{d}\xi_n}{\mathrm{d}x} + \frac{1}{\rho h}\frac{\mathrm{d}S_n}{\mathrm{d}x}\right). \tag{4.49}$$

Here $U_0 \equiv 0$ owing to the impermeable shore. Furthermore, $U_n \equiv 0$ for $n = 2, 3, 4, \ldots$, since for these n-values both ξ_n and S_n vanish so that the horizontal velocity is described by U_1 alone.

The mean energy flux W of the long-wave motion is found by taking the average over a long-wave period, $T = 2\pi/\omega$ of the linearized version of (3.5). We get

$$\begin{aligned} W &= \frac{1}{T}\int_0^T \rho g h \bar{\xi} U \,\mathrm{d}t \\ &= \frac{1}{T}\int_0^T \rho g h \left(\sum_{n=0}^{\infty} \tfrac{1}{2}(\xi_n\,\mathrm{e}^{\mathrm{i}n\omega t} + *)\right)\left(\sum_{n=0}^{\infty} \tfrac{1}{2}(U_n\,\mathrm{e}^{\mathrm{i}n\omega t} + *)\right)\mathrm{d}t \\ &= \tfrac{1}{4}\rho g h \sum_{n=0}^{\infty} (U_n \xi_n^* + U_n^* \xi_n) \\ &= \tfrac{1}{2}\rho g h\,\mathrm{Re}\{U_1 \xi_1^*\} \end{aligned} \tag{4.50}$$

where *, as before, denotes the complex conjugate of the preceding term when it stands alone, while it means the complex conjugate of the actual term when used as a superscript.

4.2.5. *Important parameters*

A non-dimensional representation is chosen to limit the number of dependent parameters for the infragravity wave solution. Let $\hat{}$ denote non-dimensional quantities and let the lengthscale for some quantities be $k_\infty^{-1} = (\omega_s^2/g)^{-1}$ as suggested by the short-wave dispersion relation. This lengthscale will be used when defining the non-dimensional versions of the depth h, the off-shore coordinate x, and the amplitude a and wavenumber k of the short waves.

As concluded in the preceeding subsection the infragravity wave motion is to the leading order in δ described by ξ_1 alone and we chose the following non-dimensional forms

$$\hat{\xi}_1 = \frac{\xi_1}{\delta a_\infty}, \quad \hat{U}_1 = \frac{U_1}{\delta \omega_s a_\infty}, \quad \hat{W} = \frac{W}{\delta^2 W_s}, \tag{4.51}$$

where W_s is the lowest-order expression for the energy flux of the short waves before breaking.

We could have chosen to eliminate the explicit dependence of $\hat{a}_\infty$ on $\hat{\xi}_1$ by the redefinition $\hat{\xi}_1 := \hat{\xi}_1/\hat{a}_\infty$. However, there would still remain an implicit dependence on the final matched solution. This dependency originates from the determination of the match point corresponding to the mean break-point depth, which is still a function of $\hat{a}_\infty$.

It turns out that in all results the bottom slope h_x only appears as part of the parameter $h_x\omega_s/\omega$. This parameter is the ratio between two small quantities, one being the bottom slope, and the other the ratio of infragravity-wave frequency to short-wave frequency $\omega/\omega_s = 2\epsilon$ (see (2.35)). Thus for a fixed (mean) short-wave frequency the solution is unchanged if the bottom slope and the difference frequency are changed by the same factor. This means that long, short-wave groups over small bottom slopes give similar infragravity-wave activity as short, short-wave groups over steep bottom slopes.

As a consequence of the choice of non-dimensional form the solution is determined by the five parameters

$$\frac{h_x\omega_s}{\omega}, \quad \hat{h}_0, \quad \hat{a}_\infty, \quad \kappa, \quad \gamma_0, \tag{4.52}$$

where h_0 is the depth in region III. In real life, however, the first three parameters in (4.52) together with h_x would suffice, and nature would provide the best fit for γ_0 and κ. However, we have chosen to keep the five parameters in (4.52) as our set of input parameters, only using the empirical information on γ_0 and κ as a guideline to their relevant magnitudes.

In order to get some quantitative measure of the magnitude of the free wave propagating seawards in region III relative to the incoming bound, long wave, we define a 'reflection coefficient' R as the ratio between their respective amplitudes

$$R = \frac{|\beta^{(\mathrm{III})}|}{|S_{\mathrm{I}}^{(\mathrm{III})}|/\rho(gh_0 - c_{g0}^2)}, \tag{4.53}$$

see (4.17). If $\hat{h}_0$ corresponds to deep water for the short waves (but still shallow water for the long waves) then the amplitude of the bound, long wave will be proportional to $(\hat{h}_0 - \frac{1}{4})^{-1}$, whereas the free, long wave will be proportional to $\hat{h}_0^{-\frac{1}{4}}$ according to Green's law. Thus the influence of depth is much weaker on the free, long wave than on the bound, long wave. We have

$$R \propto \frac{\hat{h}_0^{-\frac{1}{4}}}{(\hat{h}_0 - \frac{1}{4})^{-1}} = \frac{\hat{h}_0 - \frac{1}{4}}{\hat{h}_0^{\frac{1}{4}}} \quad \text{for } \hat{h}_0 \gtrsim 3, \tag{4.54}$$

so that R is large for large $\hat{h}_0$ – in fact $R \to \infty$ as $\hat{h}_0 \to \infty$. ($\hat{h} = 3$ corresponds to $h_0/L_s \approx 0.5$.)

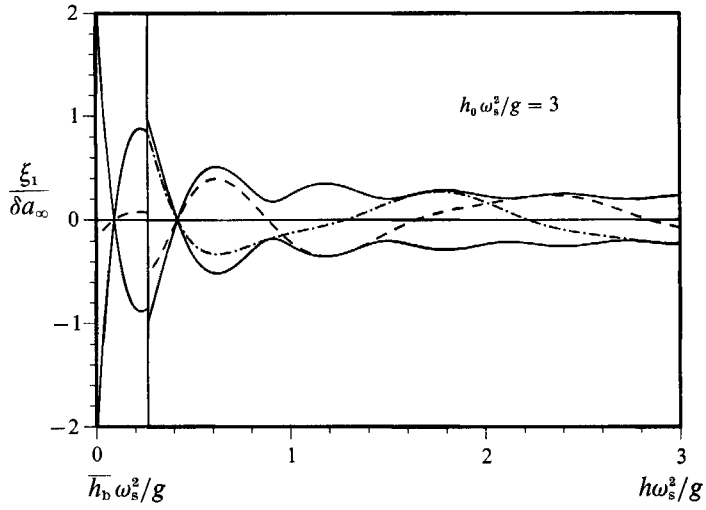

FIGURE 5. Dimensionless infragravity wave: ——, envelope $\pm|\hat{\xi}_1|$ and elevations – – –, $\mathrm{Re}\{\hat{\xi}_1\}$ at $t = 0$, and –·–, $\mathrm{Im}\{\hat{\xi}_1\}$ at $t = -\frac{1}{4}T$ versus $\hat{h}$ for the input parameters $h_x\omega_s/\omega = 0.25$, $\hat{h}_0 = 3$, $\hat{a}_\infty = 0.1$, $\kappa = 1$, and $\gamma_0 = 0.4$.

4.3. *Sample results for the infragravity wave*

4.3.1. *Surface elevation*

The solution for the non-dimensional surface elevation amplitude, $\xi_1/(\delta a_\infty)$, was integrated numerically, and the integration constants were found by numerical solution of the six linear equations.

Figure 5 shows an example of the solution for the input parameters $h_x\omega_s/\omega = 0.25$, $\hat{h}_0 = 3$, $\hat{a}_\infty = 0.1$, $\kappa = 1$, and $\gamma_0 = 0.4$. The figure shows the envelope of the infragravity waves (not to be confused with the envelope of the short waves), which is given by $\pm|\hat{\xi}_1|$. Furthermore, $\mathrm{Re}\{\hat{\xi}_1\}$ and $\mathrm{Im}\{\hat{\xi}_1\}$ are shown. These correspond to the surface elevation at times $t = 0$ and $t = -\frac{1}{4}T$, respectively, where $T = 2\pi/\omega$ is the infragravity wave period, which is identical with the group period of the short waves.

The solution shows a gradual change from a standing wave at the coastline to a seaward progressing wave in deep water (for the short waves). This trend will be investigated quantitatively below by computing the infragravity-wave energy flux. The progressive nature of the solution at large depths indicates that the outgoing free wave has a much larger amplitude than the incoming, bound, long wave, which is confirmed by a computed value of $R = 10.6$.

The depth at the mean break-point position, which for the chosen values of $\hat{a}_\infty$ and γ_0 is $\hat{h}_b = 0.264$, is marked with a vertical line in the figure. Here a jump in $\mathrm{Re}\{\hat{\xi}_1\}$ appears, whereas $\mathrm{Im}\{\hat{\xi}_1\}$ is continuous. This is consistent with (4.43), and it is a consequence of our choice of $t = 0$ as the time when the highest waves (in the short-wave group) break. Furthermore, there is a kink in the elevation at $\hat{h} = \hat{h}_b$ consistent with (4.47). This kink appears mainly in $\mathrm{Re}\{\hat{\xi}_1\}$, but also in $\mathrm{Im}\{\hat{\xi}_1\}$, as it should according to (4.47) considering (4.20).

For $\kappa = 1$ the break point oscillates just so much that there is no time-varying forcing in the surf zone (see (4.20)), and we get a free-wave solution there. Because of the reflective boundary condition at the shoreline this solution becomes $\hat{\xi}_1 \propto J_0(y')$, and the Bessel function may be recognized in the figures, its first zero being at $y' = 2.048$ or $\hat{h} = 1.45(h_x\omega_s/\omega)^2$, which for $h_x\omega_s/\omega = 0.25$ gives $\hat{h} = 0.09$.

The dimensional amplitude at the shoreline is approximately twice the deep-water short-wave modulation δa_∞.

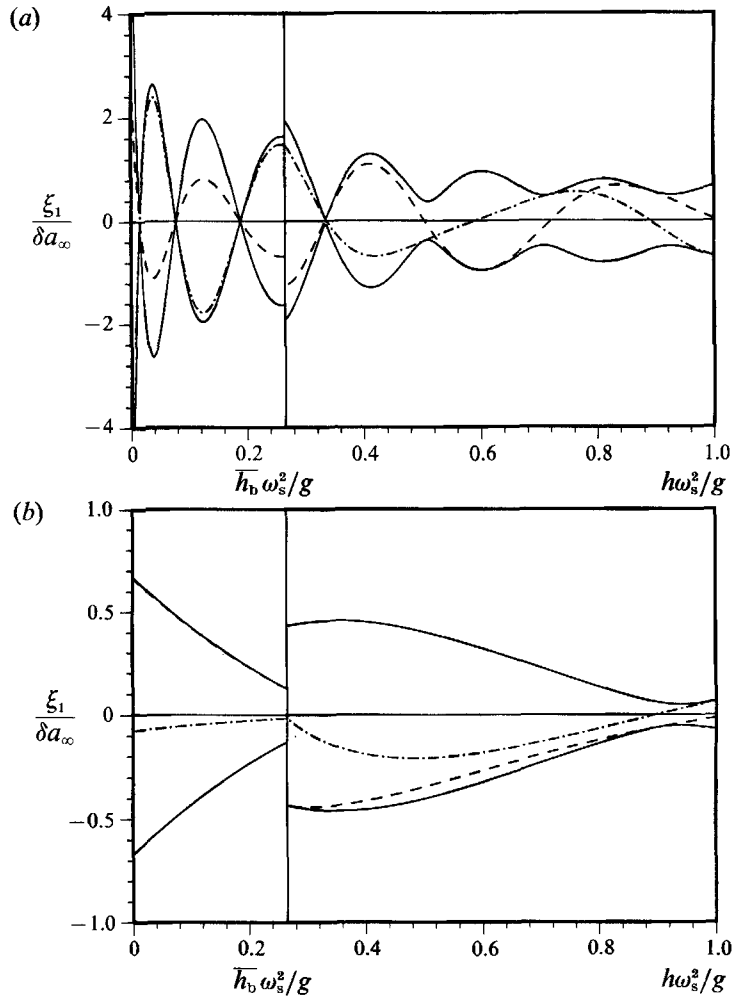

FIGURE 6. Dimensionless infragravity wave: ——, envelope $\pm|\hat{\xi}_1|$ and elevations — — —, $\mathrm{Re}\{\hat{\xi}_1\}$ at $t = 0$, and –·–, $\mathrm{Im}\{\hat{\xi}_1\}$ at $t = -\frac{1}{4}T$ versus $\hat{h}$ for the input parameters $\hat{h}_0 = 1$, $\hat{a}_\infty = 0.1$, $\kappa = 1$, $\gamma_0 = 0.4$, and (*a*) $h_x\omega_s/\omega = 0.1$ and (*b*) $h_x\omega_s/\omega = 0.5$.

Changing the depth at the shelf from the deep water value of $\hat{h} = 3.0$ to intermediate water depth $\hat{h} = 1.0$ for the short waves, leaves the solution on the slope almost unchanged, and $\hat{h} = 1.0$ is used subsequently.

The solution appears very different for different values of $h_x\omega_s/\omega$, since this parameter determines the magnitude of the arguments for the Bessel functions. Small values of $h_x\omega_s/\omega$ will give a large number of oscillations in the infragravity wave envelope and vice versa. This is demonstrated in figure 6 of which all parameters but $h_x\omega_s/\omega$ (and $\hat{h}_0$) are in common with figure 5, while $h_x\omega_s/\omega$ takes the values 0.1 and 0.5. Note the different scales on the ordinate. The figures show an increase in the infragravity-wave activity for decreasing values of $h_x\omega_s/\omega$. This also appears in the computed reflection coefficients $R = 5.0$ and $R = 1.4$, respectively. Again, we stress that the dramatic jump in the solutions at $\hat{h} = \hat{h}_b$ merely represents large gradients in the elevation over region B (the zone of initial breaking, see figure 3). This jump especially appears for $h_x\omega_s/\omega = 0.5$ for which the first zero of $J_0(y')$ lies close to the mean break-point position.

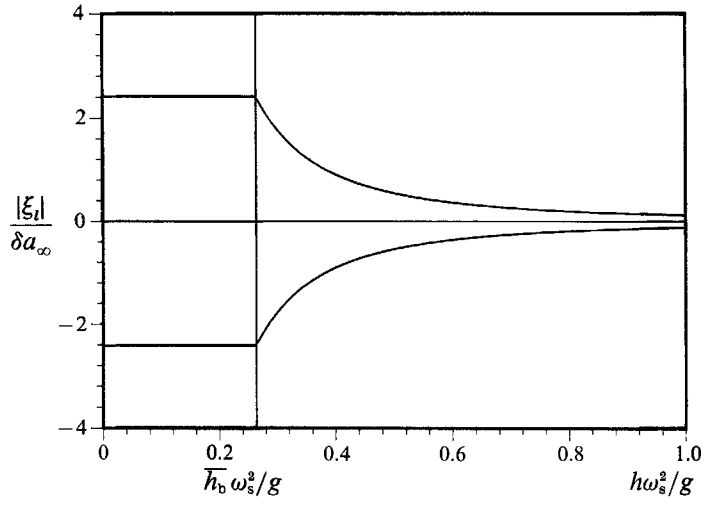

FIGURE 7. Local-solution envelope $\pm|\hat{\xi}_l|$ versus $\hat{h}$ for the input parameters $\hat{a}_\infty = 0.1$, $\gamma_0 = 0.4$, and $\kappa = 0$.

As a typical dimensional example let the short-wave period be $2\pi/\omega_s = 8\,\mathrm{s}$, the group period $T = 2\pi/\omega = 100\,\mathrm{s}$, the bottom slope $h_x = 0.02$, the modulation parameter $\delta = 0.1$ (0.2), the mean deep-water short-wave amplitude $a_\infty = 1.6\,\mathrm{m}$, and the shelf be in deep water for the short waves, then the model gives a shoreline infragravity wave amplitude of 0.3 m (0.6 m). This is for $(\kappa, \gamma_0) = (1, 0.4)$ and it corresponds to figure 5.

4.3.2. *Local solution for the bound, long wave*

In order to compare the results with a *local* solution ξ_l for the bound, long wave consider the last term in (4.17) replacing $(h_0, c_{g0}, S_I^{(III)})$ by their local values. This solution corresponds to a *geometrical optics* solution and it can only be expected to be a good approximation if the bottom slope almost vanishes. Even then it fails, in the sense that its reflection from the coastline is not incorporated. For reference $|\xi_l/\delta a_\infty)|$ is shown in figure 7 for $\hat{a}_\infty = 0.1$, $\gamma_0 = 0.4$, and $\kappa = 0$ corresponding to a constant break-point position and a full transmission of grouping into the surf zone. Note that outside the surf zone $|\xi_l|\,(\delta a_\infty)$ divided by a_∞ is independent of a_∞. The short-wave breaking is seen to limit the otherwise singular solution.

Inside the surf zone $|\xi_l|\,/(\delta a_\infty)$ appears to be almost constant. In fact, here shallow-water theory for the short waves yields

$$\frac{|\xi_l|}{\delta a_\infty} = (1-\kappa)^{\frac{3}{2}}\frac{\gamma_0^2}{\hat{a}_\infty} \quad (h < \overline{h}_b), \tag{4.55}$$

which for the parameters of figure 7 equals 2.4 consistent with the figure. Here a Taylor expansion was used correct to $O(kh)$ yielding $(c_g/c_\infty)^2 = k_\infty h(1-(kh)^2)$ by which the dimensionless denominator in the local solution becomes $\hat{h} - (c_g/c_\infty)^2 = \hat{h}^2$, applying the shallow water result, $(kh)^2 = \hat{h}$.

We now want to compare the local solution with the full solution. However these are not directly comparable, since in the full solution reflection yields a partially standing wave, while the local solution is a purely progressive wave. In order to overcome this difference we compute a new full solution, now with the artifice of substituting the reflection condition at the coastline with a condition that no free

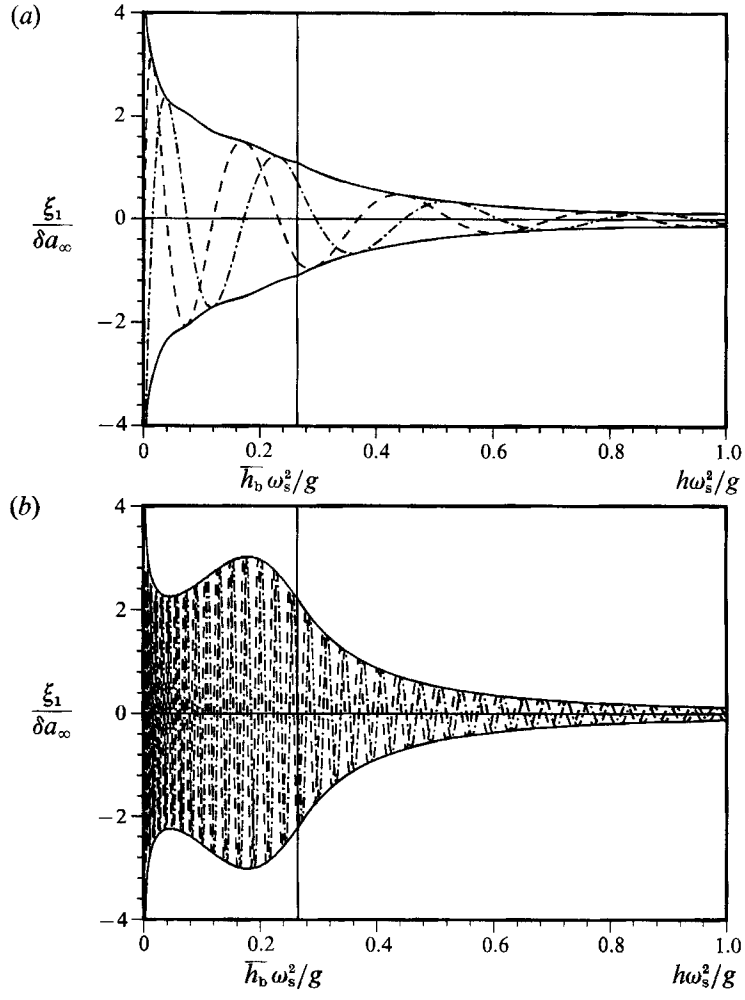

FIGURE 8. No-reflection solution: ——, envelope $\pm|\hat{\zeta}_1|$ and elevations – – –, $\mathrm{Re}\{\hat{\zeta}_1\}$ at $t = 0$, and –·–, $\mathrm{Im}\{\hat{\zeta}_1\}$ at $t = -\frac{1}{4}T$ versus $\hat{h}$ for the input parameters $\hat{h}_0 = 1$, $\hat{a}_\infty = 0.1$, $\kappa = 0$, $\gamma_0 = 0.4$, and (*a*) $h_x\omega_s/\omega = 0.1$, and (*b*) $h_x\omega_s/\omega = 0.01$.

waves progress seaward in region III. This means that there is no total reflection from the coastline and matching points $\bar{x}_b$ and x_0. Figure 8 shows this 'no-reflection' solution for $h_x\omega_s/\omega = 0.1$ and 0.01, respectively, the other parameters being $\hat{h}_0 = 1$, $\hat{a}_\infty = 0.1$, $\kappa = 0$, and $\gamma_0 = 0.4$. Comparing figure 8(*a*) with the local solution in figure 7 we see that just outside the break point the no-reflection solution yields a much smaller amplitude than the local solution; at the break point approximately 1.1 versus 2.4. Qualitatively this can be explained as the result of lack of time (or distance) for the full (no-reflection) solution to build up to the size of the local solution (which has 'local equilibrium'). Inside the surf zone figures 8(*a*) and 7 cannot be compared, since we have applied matching conditions to the no-reflection solution which are unknown to the local solution.

Changing the bottom slope or the group length in letting $h_x\omega_s/\omega$ be 0.01 as shown in figure 8(*b*) we come much closer to the local solution, since there is now more time (and distance) to build up to the size of the local solution; now we get an amplitude of 2.2 versus 2.4 for the local solution measured at the break point.

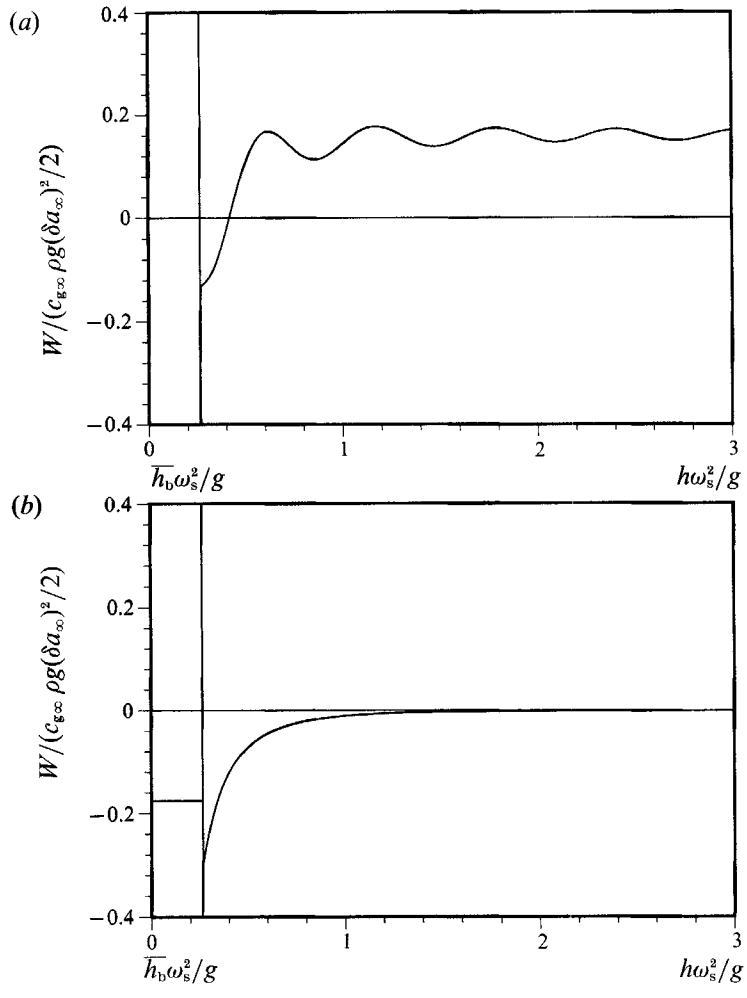

FIGURE 9. Mean infragravity-wave energy flux $\hat{W}$ versus $\hat{h}$ for the input parameters $h_x\omega_s/\omega = 0.25$, $\hat{h}_0 = 3$, $\hat{a}_\infty = 0.1$, $\kappa = 1$, and $\gamma_0 = 0.4$. (*a*) Ordinary solution (see figure 5), and (*b*) no-reflection solution.

4.3.3. *Mean energy flux and horizontal particle velocity*

As mentioned earlier, the mean energy flux W (4.50) of the infragravity wave is a quantitative measure of the degree to which the solution is a standing wave or a progressive wave. Where the energy flux is zero we have a pure standing wave solution whereas a positive (negative) value corresponds to a seaward (shoreward) progression.

Figure 9(*a*) shows $\hat{W} = W/(\delta^2 W_s)$ for the solution shown in figure 5. Within the surf zone $\hat{W} \equiv 0$ as it should be, since there is no time-varying forcing for $\kappa = 1$. Then there is a jump to a negative value just outside the mean break point position. This illustrates the forcing within region B. Not far seaward of the surf zone the outgoing free, long wave dominates the solution and the energy flux becomes positive.

For comparison figure 9(*b*) shows $\hat{W}$ for the no-reflection solution introduced above for the same input parameters. The absence of reflection gives a monotonically decreasing energy flux (of which the absolute value is increasing) as the incoming forced wave approaches the surf zone.

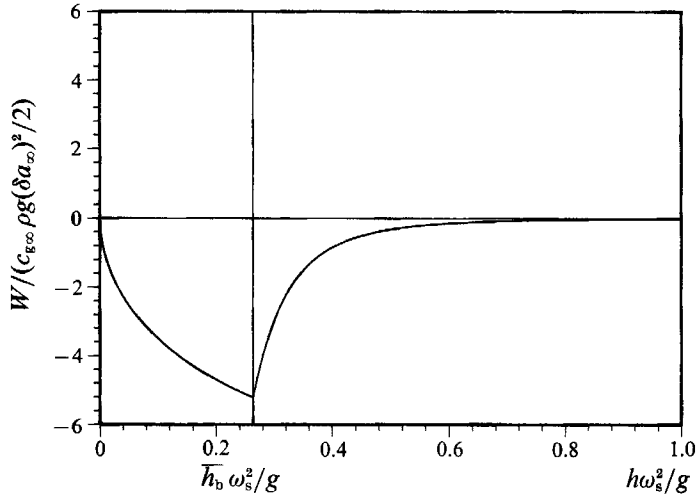

FIGURE 10. Mean infragravity-wave energy flux $\hat{W}$ versus $\hat{h}$ for the local solution $\hat{\xi}_l$ (figure 7) for the input parameters $\hat{a}_\infty = 0.1$, $\gamma_0 = 0.4$, and $\kappa = 0$.

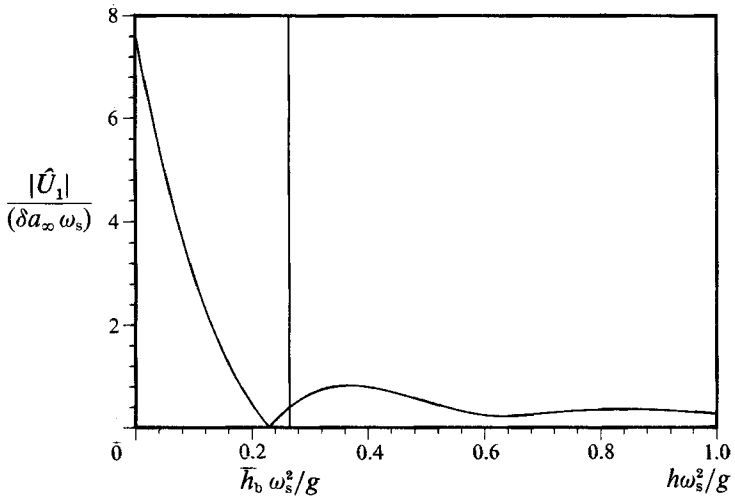

FIGURE 11. Amplitude of horizontal infragravity wave particle velocity, $|\hat{U}_1|$, versus $\hat{h}$ for the input parameters $\hat{a}_\infty = 0.1$, $\gamma_0 = 0.4$, and $\kappa = 1$.

The energy flux of the local solution (see figure 7) is shown in figure 10. As expected, this solution represents an energy flux close to the break point which is much greater than that which we have computed for our full solution. This is partly because the local solution does not include a wave reflected from the coastline, partly because the sloping bed does not allow the full solution to build up to the size of the local solution, as commented on earlier.

Figure 11 shows the non-dimensional horizontal particle velocity $|\hat{U}_1| = |U_1|/(\delta a_\infty\,\omega_s)$ for the infragravity wave shown in figure 5 (except for $\hat{h}_0 = 1$ instead of 3). Shorewards of the zero (where the surface elevation has an antinode) the velocity is seen to increase rapidly consistent with Wright *et al.* (1982), who observed large nearshore velocities at infragravity frequencies in the field.

Figure 11 supports the idea that infragravity waves are very important for the formation of nearshore bars.

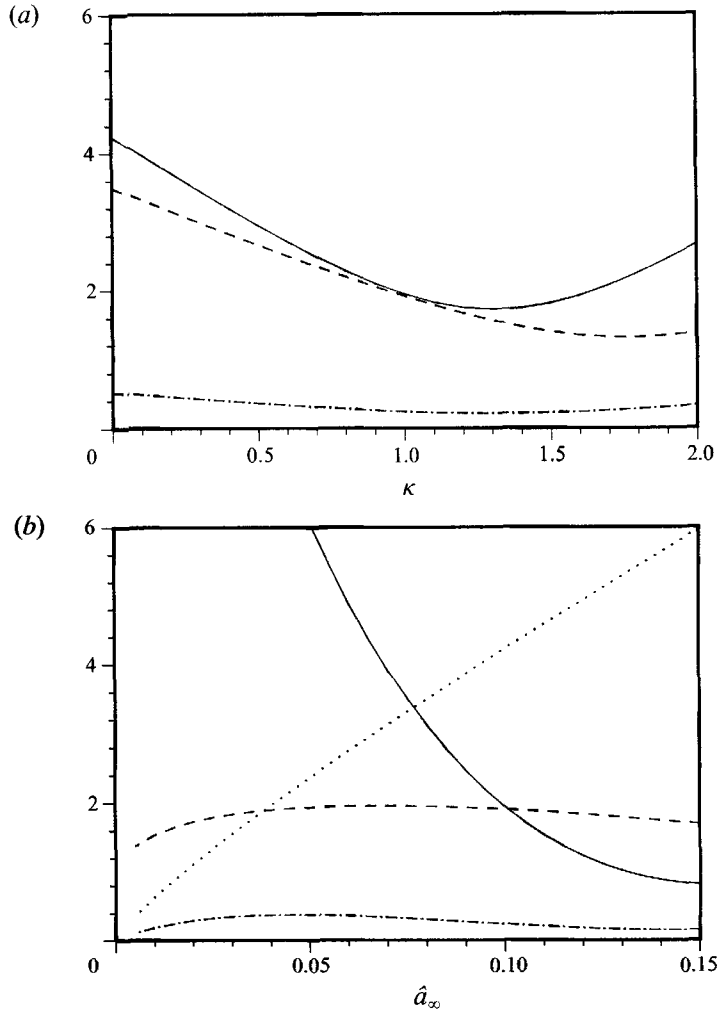

FIGURE 12. ——, 'Reflection coefficient' R; – – –, shoreline infragravity-wave amplitude $|\xi_1(0)|/(\delta a_\infty)$ and –·–, amplitude of the outgoing, free, long wave $|\xi_f|/(\delta a_\infty)$ versus (*a*) κ for $\hat{a}_\infty = 0.1$, and (*b*) $\hat{a}_\infty$ for $\kappa = 1.0$. The other input parameters were $h_x\omega_s/\omega = 0.25$, $\hat{h}_0 = 1$, and $\gamma_0 = 0.4$. Furthermore, $\chi = 4.22$ in (*a*) and ···, χ is shown in (*b*).

4.3.4. *The influence of varying input parameters*

The following quantities are chosen to represent the infragravity-wave activity: the reflection coefficient R, the infragravity-wave amplitude at the shoreline $|\xi_1(0)|/(\delta a_\infty)$, and the amplitude of the seaward progressing free wave in the shelf zone (region III) $|\xi_f|/(\delta a_\infty)$.

Figure 12(*a*) shows R, $|\xi_1(0)|/(\delta a_\infty)$, and $|\xi_f|/(\delta a_\infty)$ versus κ, the rest of the input parameters being $h_x\omega_s/\omega = 0.25$, $\hat{h}_0 = 1$, $\hat{a}_\infty = 0.1$, and $\gamma_0 = 0.4$. Note that here $R \propto |\xi_f|/(\delta a_\infty)$, since $\hat{h}_0$ and $\hat{a}_\infty$ are fixed. χ is defined below. Referring to the discussion closing §2.2.2, κ is probably not far from unity and the range $0 \leqslant \kappa \leqslant 2$ used in figure 12(*a*) is not physically realistic. However, the figure still illustrates the significance of κ. As mentioned earlier we have made the choice that at $t = 0$ the incident short-wave groups have a maximum at the mean break-point position, carrying with them

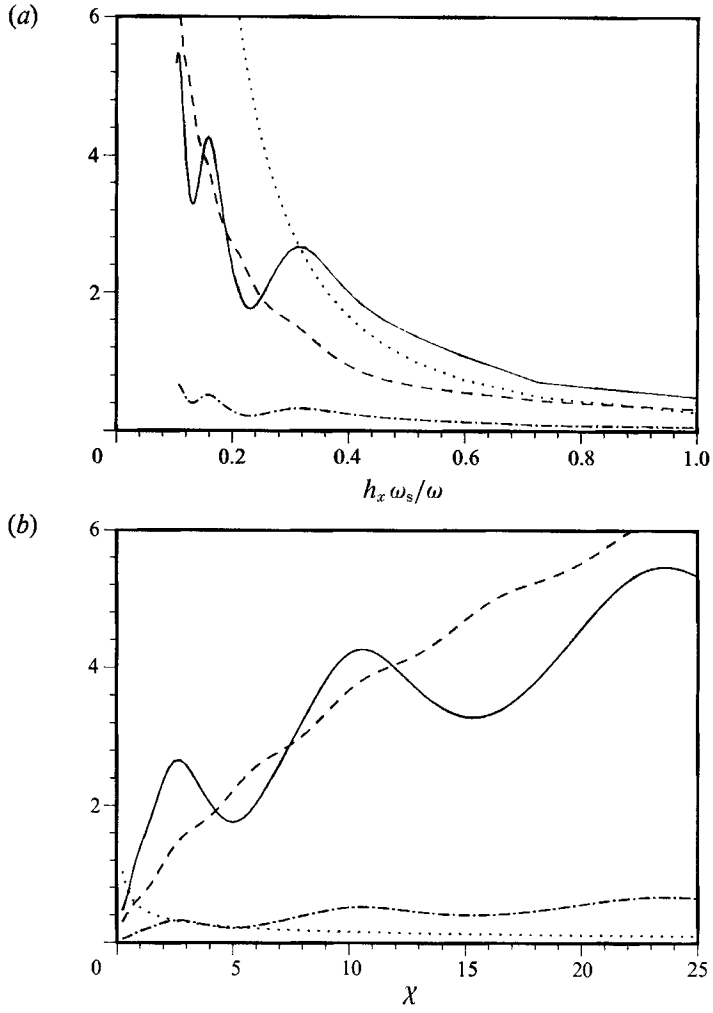

FIGURE 13. ——,'reflection coefficient' R; – – –, shoreline infragravity-wave amplitude $|\xi_1(0)|/(\delta a_\infty)$; and – · –, amplitude of the outgoing, free, long wave $|\xi_f|/(\delta a_\infty)$ versus (*a*) $h_{x_s}\omega_s/\omega =$, and (*b*) χ. (*a*) and (*b*) represent the same information. The other input parameters were $\hat{h}_0 = 1$, $\hat{a}_\infty = 0.1$, $\kappa = 1$, and $\gamma_0 = 0.4$. Furthermore, χ (· · · · · ·) is shown in (*a*), and $h_x\omega_s/\omega$ (· · · · · ·) is shown in (*b*).

a depression of the mean water surface. For any (positive) κ-value the jump condition (4.43*a*) counteracts this depression. Physically the explanation is that groups of high, short waves carry with them a set-down, which is opposed by the larger set-up that they also tend to produce.

The value of $\kappa = 1$ represents a qualitative turning point. For $\kappa > 1$ the forcing is reversed inside the surf zone favouring the set-up effect, whereas for $\kappa < 1$ the set-down effect is reinforced.

Altogether this means that we may expect the infragravity-wave activity (for example measured by one of the quantities R, $|\xi_1(0))|/(\delta a_\infty)$ or $|\xi_f|/(\delta a_\infty)$) to have a minimum for some κ-value of the order of one, since for $\kappa = 0$ (fixed break-point position) nothing opposes the dynamic set-down, whereas for a large κ the dynamic set-up is predominant. This is confirmed by figure 12(*a*).

Figure 12(*b*) shows R, $|\xi_1(0)|/(\delta a_\infty)$, and $|\xi_f|/(\delta a_\infty)$ versus $\hat{a}_\infty$ for $h_x\omega_s/\omega = 0.25$, $\hat{h}_0 = 1$, $\kappa = 1.0$, and $\gamma_0 = 0.4$. For reference the figure also shows the parameter χ, see below. Note that the modelling of the short waves in the surf zone more or less assumes spilling breakers. This requires $\hat{a}_\infty \gtrsim 0.05$ even for very small slopes.

The non-dimensional shoreline amplitude is almost independent of the short-wave steepness and the non-dimensional seaward progressing free wave is even decreasing for increasing $\hat{a}_\infty$. This means that the physical infragravity wave activity has a roughly linear (or weaker) dependence on the short-wave amplitude. This is in line with the early observations by Munk (1949) and Tucker (1950) and the more recent observations by Guza & Thornton (1982, 1985). Thus the model does not show the quadratic dependency on the short-wave amplitude which has been a problem with earlier qualitative explanations for infragravity waves relying solely on the local solution for the bound, long wave.

Figure 13(*a*) shows R, $|\xi_1(0)|/|a_\infty)$, and $|\xi_f|/(\delta a_\infty)$ (and χ) versus $h_x\omega_s/\omega$ for $\hat{h}_0 = 1$, $a_\infty = 0.1$, $\kappa = 1$, and $\gamma_0 = 0.4$. The trend of a reflection coefficient increasing rapidly with decreasing $h_x\omega_s/\omega$ is seen to be distorted by large oscillations. These oscillations are due to the phase difference between two essentially free, long waves, both of which are generated in the region of initial breaking, one being subject to direct seaward emission and the other being emitted after reflection from the shoreline. Figure 13(*b*) represents the same data as figure 13(*a*) only now as function of

$$\chi \equiv \frac{\omega^2\bar{x}_b}{g\hat{h}_x} = \left(\frac{h_x\omega_s}{\omega}\right)^{-2}\hat{h}_b = (\tfrac{1}{2}\bar{y}'_b)^2 \tag{4.56}$$

introduced by Symonds *et al.* (1982) as a measure of the relative phase just mentioned.

Solutions for a wider range of parameters are shown in Schäffer (1990).

4.4. *Comparison with the theoretical results of Symonds* et al. *(1982)*

As mentioned in the introduction, Symonds *et al.* (1982) were the first to develop a model for infragravity waves forced by oscillations in the break-point position. In this pioneering work, however, they neglected all forcing effects outside the zone of initial breaking, region B (see figure 3), and thus the incident bound, long wave was not a part of their solution. Furthermore, they assumed that all the short-wave grouping was destroyed in producing the time-varying break-point position. This corresponds to the value $\kappa \equiv 1$ (the parameter introduced in §2.2.2) which is not far from our estimate of $\kappa \sim 1.1$, though. Reformulating the jump conditions (4.43) according to these assumptions we obtain

$$\left.\begin{aligned}\left[\frac{2\xi_1}{3\gamma_0^2\bar{x}_b h_x}\right]_-^+ &= -\delta \\ \left[\frac{2\xi_n}{3\gamma_0^2\bar{x}_b h_x}\right]_-^+ &= 0 \quad (n = 2,3,4,\ldots)\end{aligned}\right\} \quad (x = \bar{x}_b), \tag{4.57}$$

where also shallow-water theory was applied. These questions give the jump over region B in the non-dimensional form of Symonds *et al.* Furthermore, the kink conditions (4.47) vanish under the given assumptions. Thus to the leading order in δ their solution is found solely by matching free long-wave solutions (a standing wave in the surf zone represented by a Bessel function and a seawards propagating wave outside the surf zone represented by a Hankel function) requiring a jump $-\delta$ at the

Series	$a_0^{(1)}$ (cm)	$a_0^{(2)}$ (cm)	$\omega^{(1)}$ (rad/s)	$\omega^{(2)}$ (rad/s)	ω (rad/s)	χ
*A*1	5.5	1.1	3.062	2.145	0.917	5.81
*A*2	5.5	1.1	3.062	2.296	0.766	4.05
*A*3	5.5	1.1	3.065	2.456	0.609	2.55
*A*4	5.5	1.1	3.077	2.618	0.459	1.44
*A*5	5.5	1.1	3.063	2.755	0.308	0.65
*B*1	5.5	1.1	4.295	3.372	0.923	5.57
*B*2	5.5	1.1	4.065	3.293	0.772	3.93
*B*3	5.5	1.1	4.070	3.455	0.615	2.48
*B*4	5.5	1.1	4.071	3.609	0.462	1.39
*B*5	5.5	1.1	4.070	3.762	0.308	0.62
*C*1	8.0	1.6	4.294	3.522	0.772	5.33
*C*2	5.5	1.1	4.065	3.293	0.772	3.93
*C*3	3.5	0.7	4.295	3.523	0.772	2.65
*D*1	5.5	1.1	3.065	2.456	0.609	2.55
*D*2	3.5	0.7	3.065	2.456	0.609	1.76
*D*3	3.0	0.6	3.065	2.456	0.609	1.55

TABLE 1. Short-wave characteristics for the experiments by Kostense (1984). The listed χ-values (based on $\gamma_0 = 0.4$) differ a little from the ones used by Kostense, owing to his neglect of short-wave shoaling.

mean break-point position. A thorough comparison with the theory of Symonds *et al.* is given in Schäffer (1990).

4.5. *Comparison with laboratory experiments by Kostense (1984)*

A series of high-quality laboratory experiments on long waves forced by short-wave groups, conducted at the Delft Hydraulics Laboratory, we reported by Kostense in 1984. Fortunately his experimental set-up exactly meets the assumptions behind the present theoretical model. This applies to the bottom profile as well as to the incident short-wave groups, and his measurements include the respective amplitudes of the incident, bound, long wave and the seaward progressive, free, long wave. The movement of the wave-maker paddle included second-order generation as well as active absorption of free, long waves returning to the wavemaker. Consequently, standing waves arising from the reflection of free, long waves at the paddle were avoided, and the measurements provide an excellent test of the present theory.

Five series of experiments are reported, and the first four of these correspond to a short-wave modulation parameter of $\delta = 0.2$. This meets our assumptions of $\delta \ll 1$, considering the limited accuracy expected from the theoretical model owing to the complicated physical mechanisms in question. The characteristics of the incident short waves for these four series (*A*–*D*) are given in table 1. Here $(a_0^{(1)}, a_0^{(2)})$ and $(\omega^{(1)}, \omega^{(2)})$ are the amplitudes (over the shelf) and angular frequencies of the two wave trains, ω is the difference frequency (group frequency), and χ is the parameter defined by (4.56). In the fifth experimental run δ equals 0.8, and no comparison is made.

The relevant parameters describing the geometry of the experimental facility are the depth $h_0 = 0.5$ m on the shelf and the beach slope $h_x = 0.05$.

In series *A* and *B* the short-wave amplitudes are kept constant while the difference frequency ω is changed, and vice versa in series *C* and *D*. The resulting amplitude of

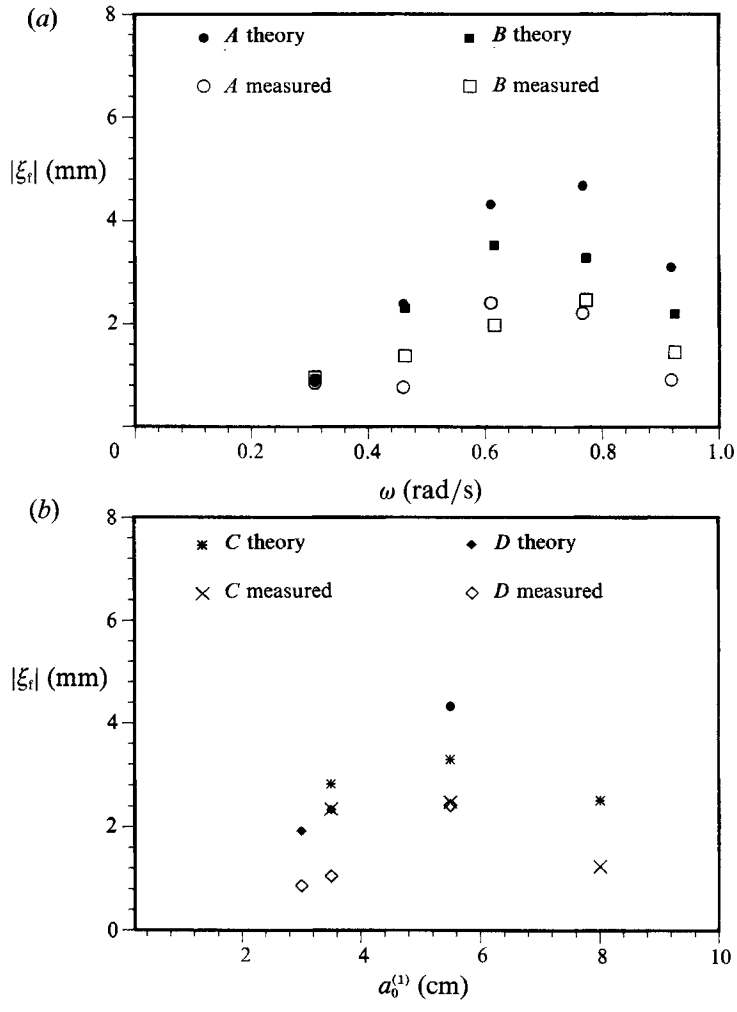

FIGURE 14. Amplitude of outgoing free, long wave $|\xi_f|$ versus (a) the difference frequency ω (series A and B), and (b) the amplitude of the largest short-wave component $a_0^{(1)}$ (series C and D). $(\gamma_b, \kappa) = (0.4, 1.0)$.

the incident, bound, long wave $|\xi_b|$ compares very well with theory (Figure 4.22, Schäffer 1990). The excellent agreement is indeed a manifestation of the thoroughness of the experiments. The theory of the bound, long wave (also contained in the present theory) is due to Longuet-Higgins & Stewart (1962, 1964). Kostense presents a similar comparison based on an equivalent formulation given by Ottsen Hansen (1978).

We now turn to the results for the amplitude of the outgoing, free, long wave $|\xi_f|$, the generation of which is far more complex. The physical mechanisms of generation involve complicated surf zone dynamics, and thus the results of the mathematical model can hardly be expected to match the measurements as closely as the results for the bound, long wave. Two aspects of the model may be expected to give a one-sided error, one being the neglect of frictional effects, and the other the neglect of energy feed-back to the short waves. The primary consequence of the lack of energy feed-back is an overestimation of the radiation stress giving too large a

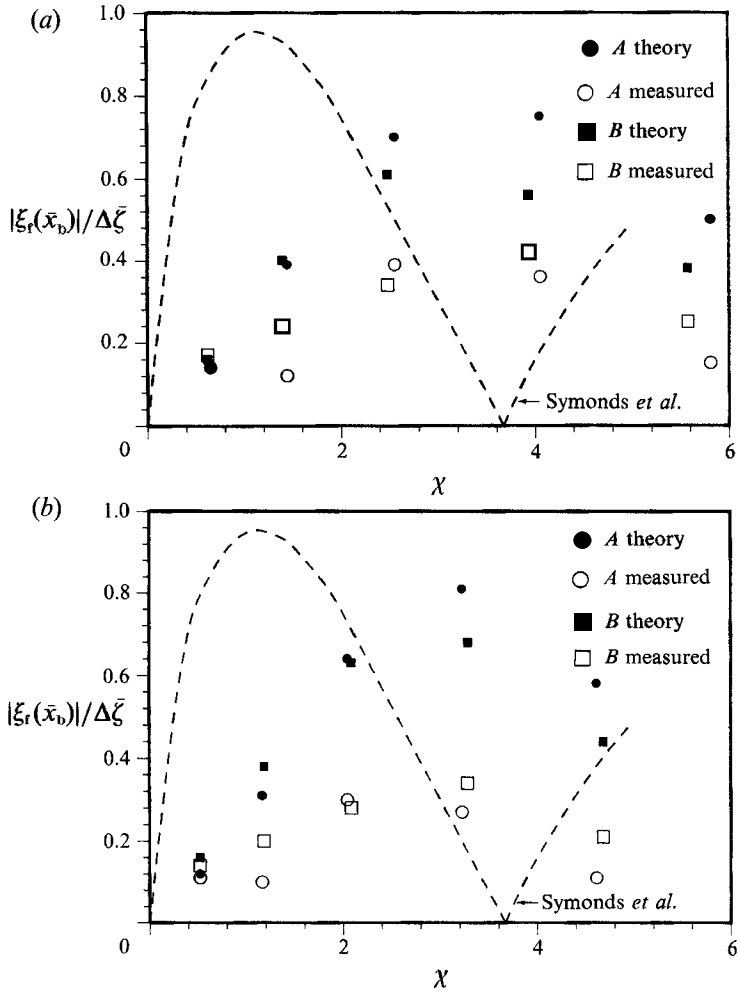

FIGURE 15. Normalized amplitude of outgoing, free, long wave $|\xi_f(\bar{x}_b)|/\Delta\bar{\zeta}$ at the mean initial break-point position versus χ for series A, and B. Comparison with the theory of Symonds *et al.* (1982) (---). (*a*) $(\gamma_0, \kappa) = (0.4, 1.0)$ and (*b*) $(\gamma_0, \kappa) = (0.47-0.53, 1.09)$ as given by the dashed curve for $h_x = \frac{1}{20}$ in figure 4.

forcing of both the dynamic set-down and the dynamic set-up. On top of this, friction affects the wave field as a whole. These arguments are slightly blurred by the fact that the infragravity wave is an interference pattern of which the components may be more or less affected by one of both of the above mentioned aspects. Still we can expect the model to generally overestimate the long-wave activity.

Figure 14 compares $|\xi_f|$ (at the shelf) from the theory and measurements, and the qualitative agreement is seen to be good. Furthermore, we recognize the expected overestimation, which for most runs is approximately 50–100%.

In order to compare with the theory of Symonds *et al.* (1982) we have used Green's law to assign the computed as well as the measured values of $|\xi_f|$ to their values $|\xi_f(\bar{x}_b)|$ at the break point. Furthermore, $|\xi_f(\bar{x}_b)|$ was normalized by the variation about the mean of the stationary shoreline set-up for infinitely long groups, denoted $\Delta\bar{\zeta}$. The results are shown in figure 15(*a*). The figure also shows the theoretical curve of

Symonds *et al.*, which is seen to be inadequate. Here $(\gamma_0, \kappa) = (0.4, 1.0)$ was used. Figure 15(*b*) is equivalent to figure 15(*a*), only the results are based on (2.47), which gives γ_0-values ranging from 0.47 to 0.53 and $\kappa = 1.09$. The general picture is seen to be the same, although the overestimation at some points is slightly larger for $\kappa = 1.09$. This is, however, due to an increase in the γ_0-values rather than the change in κ. For $\kappa = 1.09$ and $\gamma_0 = 0.4$ (not shown) a slightly better accordance with measurements is obtained. Generally, larger γ_0-values give smaller breaker depths resulting in an increase in the bound, long wave contribution as well as an increase in the dynamic set-up, their sum being affected by the change of phase difference given through χ.

For the experimental results Kostense showed that the correlation between $|\xi_f|$ and $|\xi_b|$ is very poor (as could be expected). This also applies to our theoretical results, see Schäffer & Jonsson (1990).

The theoretical $|\xi_f|$-values of this section were calculated with the assumptions of full long-wave reflection from the coastline. Introducing partial shoreline reflection (see §4.5 of Schäffer 1990) gives a 10% reduction of the theoretical $|\xi_f|$-value in the first run of series *A*, the rest of the runs being unchanged. Thus no conclusions are changed.

Kostense mentions three possible reasons for the limited validity of the theory by Symonds *et al.* These are the neglect of the incident, bound, long wave, the preclusion of short-wave grouping inside the surf zone, and the assumption of full long-wave reflection at the shoreline. The present model accounts for all these effects, and particularly inclusion of the incident, bound, long wave is of great importance. The next step towards a correct mathematical model should be the inclusion of energy feed-back to the short waves and frictional effects such as turbulence in the surf zone and bottom friction.

5. Conclusions

A theoretical model for infragravity waves generated by normally or obliquely incident short-wave groups over a one-dimensional topography has been established. For the special case of normal incidence on a plane sloping beach the solutions have been presented.

In addition to the incident, bound, long wave the model accounts for the time-varying position of the initial break point as well as a (partial) transmission of grouping into the surf zone. The break-point oscillations produce a dynamic set-up, while the weak short-wave grouping in the surf zone gives a forcing equivalent to the one that takes place outside the surf zone. The amplitude of the break-point oscillations and the degree of transmission of short-wave grouping have a mutual dependence which is modelled by a parameter κ, and for physically relevant κ-values the effect of grouping in the surf zone is inferior to the dynamic set-up. Furthermore, the dynamic set-up and the incident, bound, long wave are shown to be of almost equal importance, and it is found that they counteract each other to some extent. This is physically comprehensible, since we can regard the incident, bound, long wave as a dynamic set-down.

The parameter κ is determined by the extent of the break-point oscillations owing to the short-wave grouping. To this end no experimental data are available, and experiments are needed. However, an estimate of κ has been obtained from experimental results for regular waves.

The solution for the infragravity wave exhibits a roughly linear (or weaker) dependence on the short-wave steepness. This is in accordance with field observations and it contradicts earlier qualitative explanations for infragravity waves relying solely on second-order progressive wave theory.

The model is in qualitative agreement with laboratory experiments, and even the quantitative results are fairly good considering that frictional effects are neglected.

Professor I. G. Jonsson is gratefully acknowledged for stimulating discussions and comments, and for his help with the preparation of this manuscript. Furthermore, I am indebted to Professor I. A. Svendsen, who introduced me to the field of wave hydrodynamics and also initiated the present research. This work was conducted while I was a research student at the Institute of Hydrodynamics and Hydraulic Engineering, Technical University of Denmark.

REFERENCES

ABRAMOWITZ, M. & STEGUN, I. A. 1972 *Handbook of Mathematical Functions*. Dover, New York.

BOWERS, E. C. 1977 Harbour resonance due to set-down beneath wave groups. *J. Fluid Mech.* **79**, 71–93.

CARRIER, C. F. & GREENSPAN, H. P. 1958 Water waves of finite amplitude on a sloping beach. *J. Fluid Mech.* **4**, 97–109.

CHU, V. H. & MEI, C. C. 1970 On slowly varying Stokes waves. *J. Fluid Mech.* **41**, 873–87.

GODA, Y. 1970 A synthesis on breaker indices. *Trans. Japan Soc. Civ. Engrs* **2**, (2), 227–230.

GUZA, R. T. & THORNTON, E. B. 1982 Swash oscillations on a natural beach. *J. Geophys. Res.* **87**, C1, 483–491.

GUZA, R. T. & THORNTON, E. B. 1985 Observations of surf beat. *J. Geophys. Res.* **90**, C2, 3161–3171.

HANSEN, J. B. 1990 Periodic waves in the surf zone: analysis of experimental data. *Coastal Engng* **14**, 19–41.

KOSTENSE, J. K. 1984 Measurements of surf beat and set-down beneath wave groups. *Proc. 19th Intl Conf. Coastal Engng, Houston, Texas, 1984*, vol. 1, pp. 724–40. ASCE, New York, 1985.

LIU, P. L.-F. 1989 A note on long waves induced by short-wave groups over a shelf. *J. Fluid Mech.* **105**, 163–170.

LIST, J. H. 1991 Wave groupiness variations in the nearshore. *Coastal Engng* **15**, 475–496.

LO, J.-M. 1988 Dynamic wave setup. *Proc. 21st Intl Conf. Coastal Engng, Malaga, Spain, 1988*, vol. 2, pp. 999–1010. ASCE, New York, 1989.

LONGUET-HIGGINS, M. S. & STEWART, R. W. 1962 Radiation stress and mass transport in gravity waves with application to 'surf beats'. *J. Fluid Mech.* **13**, 481–504.

LONGUET-HIGGINS, M. S. & STEWART, R. W. 1964 Radiation stresses in water waves: a physical discussion with applications. *Deep Sea Res.* **11**, 529–562.

MEI, C. C. 1983 *The Applied Dynamics of Ocean Surface Waves*. Wiley.

MEI, C. C. & AGNON, Y. 1989 Long period oscillations in harbours induced by incident short waves. *J. Fluid Mech.* **208**, 595–608.

MEI, C. C. & BENMOUSSA, C. 1984 Long waves induced by short-wave groups over an uneven bottom. *J. Fluid Mech.* **139**, 219–235.

MEYER, R. E. & TAYLOR, A. D. 1972 Run-up on beaches. In *Waves on Beaches*. (ed. R. E. Meyer), pp. 357–412. Academic.

MOLIN, F. 1982 On the generation of long-period second-order free-waves due to changes in the bottom profile. *Ship. Res. Inst. Papers*, vol. 68. Tokyo.

MUNK, W. H. 1949 Surf beats. *Trans. Am. Geophys. Union* **30**, 849–854.

NAKAZA, E. & HINO, M. 1991 Bore-like surf beat in a reef caused by wave groups of incident short period waves. *Fluid dyn. Res.* **7** (Jap. Soc. of Fluid Mech.), 89–100.

OTTESEN HANSEN, N.-E. 1978 Long period waves in natural wave trains. *Prog. Rep.* **46**, 13–24. Inst. Hydrodyn. Hydr. Engng (ISVA), Technical University of Denmark.

PHILLIPS, O. M. 1977 *The Dynamics of the Upper Ocean*, 2nd edn. Cambridge University Press.

ROELVINK, J. A. 1991 Modelling of cross-shore flow and morphology. *Proc. Coastal Sediments '91, Seattle, USA*, vol. 1, pp. 603–617. ASCE, New York 1991.

SAND, S. E. 1982 Long wave problems in laboratory models. *J. Waterway, Port, Coastal and Ocean Div., Proc. ASCE*, **108**, 492–503.

SCHÄFFER, H. A. 1990 Infragravity water waves induced by short-wave groups. PhD thesis. Series paper 50, Inst. Hydrodyn. Hydr. Eng. (ISVA), Technical University of Denmark, 168 pp.

SCHÄFFER, H. A. 1993 Laboratory wave generation correct to second order. *Proc. Intl Conf. Wave Kinematics and Environmental Forces, London, England, 1993.* Soc. Underwater Tech.

SCHÄFFER, H. A. & JONSSON, I. G. 1990 Theory versus experiments in two-dimensional surf beats. *Proc. 22nd Intl Conf. Coastal Engng, Delft, The Netherlands 1990*, vol. 2, pp. 1131–1143. ASCE, New York, 1991.

SCHÄFFER, H. A., JONSSON, I. G. & SVENDSEN, I. A. 1990 Free and forced cross-shore long waves. In *Water Wave Kinematics* (ed. A. Tørum & O. T. Gudmestad), pp. 367–385. Kluwer Academic Publishers, Dordrecht.

SCHÄFFER, H. A. & SVENDSEN, I. A. 1988 Surf beat generation on a mild slope beach. *Proc. 21st Intl Conf. Coastal Engng, Malaga, Spain, 1988*, vol. 2, pp. 1058–1072. ASCE, New York, 1989.

SVENDSEN, I. A. 1984 Wave heights and set-up in a surf zone. *Coastal Engng* **8**, 303–329.

SYMONDS, G. & BOWEN, A. J. 1984 Interactions of nearshore bars with incoming wave groups. *J. Geophys. Res.* **89**, C2, 1953–1959.

SYMONDS, G., HUNTLEY, G. A. & BOWEN, A. J. 1982 Two dimensional surf beat: long wave generation by a time-varying break point. *J. Geophys. Res.* **87**, C1, 492–498.

TUCKER, M. J. 1950 Surf beats: sea waves of 1 to 5 min. period. *Proc. R. Soc. Lond.* A **202**, 565–573.

VAN LEEUWEN, P. J. & BATTJES, J. A 1990 A model for surf beat. *Proc. 22nd Intl Conf. Coastal Engng, Delft, The Netherlands 1990*, vol. 1, pp. 32–40. ASCE, New York, 1991.

WRIGHT, L. D., GUZA, R. T. & SHORT, A. D. 1982 Surf zone dynamics on a high energy dissipative beach. *Mar. Geol.* **45**, 41–62.

WU, J.-K. & LIU, P. L.-F. 1990 Harbour excitations by incident wave groups. *J. Fluid Mech.* **217**, 595 613.